PROCESSING AND FERROELECTRIC PROPERTIES OF $Pb_{0.91}Sr_{0.09}(Zr_{0.53}Ti_{0.47})O_3$ CERAMICS

By

Muhammad Khalid

Submitted to the Department of Materials Engineering,
School of Chemical and Materials Engineering (SCME),
in partial fulfillment of the requirements for the degree of
Masters in Materials & Surface Engineering

National University of Sciences and Technology
Islamabad, Pakistan

July, 2008

This work is dedicated to my parents

ABSTRACT

Lead Zirconate Titanate (PZT) with formulae $Pb_{0.91}Sr_{0.09}(Zr_{0.53}\ Ti_{0.47})O_3$ was prepared by conventional mixed oxide route with an objective to achieve dense piezoelectric sintered components exhibiting adequate properties for sonar applications. Dielectric and ferroelectric/piezoelectric properties of PZT are strongly influenced by composition, homogeneity and porosity in the densified part. To achieve the objective of a good homogenous and dense body, the initial powders and the final product were characterized by SEM equipped with EDX, XRD and Particle Size Analyzer during each processing step. Electrical characterization was carried out by LCR meter and Transducer Analyzer. Planetary Mill instead of a conventional ball mill was employed for initial mixing and grinding of calcined powder. Properties achieved by sintering at 1200°C for 2 hours in lead rich atmosphere were Dielectric Cosntant (K) = 1440, Tangent Loss (Tanδ) = 0.0062, Charge Coefficient(d_{33}) = 335 pC/N, Coupling Coefficient (k) = 0.37 and density = 7.55 g/cm^3. XRD analysis of calcined powders showed that excess PbO added at the time of preparation of the mixture started to evaporate at the calcination stage. After sintering the observed grain size was 2-3 µm with clean grain boundaries. To ascertain the effects of accelerated ageing on dielectric and piezoelectric properties, final product was first heated at 50°C for 5 days and then at 100°C for 3 days. The results showed that dielectric and piezoelectric properties were stabilized to a large extent by heating at 100°C for 3 days. The ageing data for 9% Sr doped PZT is not reported earlier, therefore, it would help in great deal in predicting the performance of component in service.

ACKNOWLEDGEMENTS

No work can be done in isolation and this thesis is no exception.

First of all I would like to pay my gratitude to my parent department for allowing me to start my MS leading to PhD Program sponsored by Higher Education Commission (HEC) of Pakistan.

I am also thankful to my supervisor Dr. Amir Azam Khan for his support and positive criticism. He always encouraged me in developing critical thinking not only for this project but also in other scientific areas.

My gratitude also goes to my Co-Supervisor Dr. Muhammad Shoaib for his guidance and technical help in processing of PZT ceramics. I have learnt a lot about piezoelectricity by working with him.

Great thanks also to my colleague Mr. Saleem Mirza for his help in measurement of dielectric and piezoelectric properties and for literature support. He always shared his knowledge with me. I am obliged to Mr. Abdul Rauf in encouraging working in strontium doped PZT ceramics and to Mr. Shakir for his technical cooperation and providing chemicals and basic hardware. Ms. Fareeda Yasmeen helped in SEM and EDX analysis. Wonderful SEM micrographs that will be observed in the present work would not have been possible without her help.

I would also acknowledge Dr. Muhammad Islam, Mr. Muhammad Faisal, Mr. Khalid Mahmood, Mr. Mudussar, Dr. Amir Nusair, Mr. Wali Muhammad, Mr. Saif Ullah Awan, Mr. Shahid Mehboob, Mr. Khalid Akbar, Mr. Noveed, Mr. Arshad and Mr. Munir for their technical help and support.

And at the last I pay my sincere thanks to my wife who sacrificed a lot since the day I started my MS programme and she always encouraged me in difficult hours.

TABLE OF CONTENTS

1 Introduction

The piezoelectric effect was first discovered in 1880 by Pierre and Jacques Curie in naturally occurring crystals such as quartz and Rochelle salt. The first significant application for piezoelectrics occurred during world war-1, when Langevin developed a means of generating acoustic waves in water for signaling and detection of German submarines. These early forms of active sonar employed the use of piezoelectric quartz. In 1920, ferroelectric behavior was discovered in Rochelle salt by Joseph Valasek. Because of its large piezoelectric effect, Rochelle salt became widely used in microphones, phonographs, loudspeakers, recorders, and oscillographs. In 1930, Sawyer and Tower developed a circuit to record the hysteresis behavior of this ferroelectric. The first polycrystalline piezoelectric, based on $BaTiO_3$, was discovered by Von Hippel and others in the mid 1940s. R.B. Gray and S. Roberts were among the first to develop piezoelectric ceramics by "Poling" ferreolectrics. The ferroelectric behavior o f lead titanate was discovered in 1950. In 1952, piezoelectric behavior was discovered in tungsten-bronze structure lead niobate. In the mid 1950s, PZT, (lead zirconate titanate) was developed and became the most widely used piezoelectrics ceramics to date. The first piezoelectric polymer, polyvinyledene fluoride, was developed in 1969 by stretching it under high fields. More recently, a variety of complex niobate based piezoelectric with very high piezoelectric coefficients have been developed. Multilayer and thin film processing have dramatically expanded the application of this important group of materials.[1]

Polycrystalline piezoelectric materials exhibiting ferroelectric behavior are the center of attention, because they can be readily formed into various shapes and sizes using conventional processing. Ferro electricity is the spontaneous alignment of dipoles as a result of their mutual interaction. At lower temperatures, the electric dipoles in a ferroelectric material create a local field that is stronger than the thermal energy required for randomizaion and spontaneous polarization results. Without external applied forces, the dipoles align in regions or domains. The various domains are then oriented along different crystallographic directions resulting in the lowest (strain) energy state and a net-zero polarization for the sintered ceramic compounds with perovskite structure .These include $Pb(Zr,Ti)O_3$ (PZT), $BaTiO_3$, $Pb(Mg_{1/3}Nb_{2/3})O_3$ PMN, and Pb $(Zn_{1/3}Nb_{2/3})O_3$ PZN. In addition tungsten–bronze structure such as (Sr, Ba) Nb_2O_6, and $LiNb_2O_6$ are often ferroelectric.

Since the discovery of ferro-electricity in single-crystal materials (Rochelle salt) in 1921 and its subsequent extension into the realm of polycrystalline ceramics (barium titanate, $BaTiO_3$) during the early to mid-1940s, there has been a continuous succession of new materials and technology developments that have led to a significant number of industrial and commercial applications that can be directly credited to this most unusual phenomenon. Among these applications are high dielectric-constant capacitors, piezoelectric sonar and ultrasonic transducers, radio and communication filters, pyroelectric security surveillance devices, medical diagnostic transducers, stereo tweeters, buzzers, gas igniters, positive temperature coefficient (PTC) sensors and switches, ultrasonic motors, electro optic light valves, thin-film capacitors, and ferroelectric thin-film memories. $Pb_{0.91}Sr_{0.09}(Zr_{0.53},Ti_{0.47})O_3$ ceramic is one of the many compositional variations of Lead Zirconate Titinate (PZT) ceramics systems. PZT ceramics are special type of dielectric materials.

Ferroelectric ceramics for piezoelectric applications historically have been formulated from a number of compositions and solid solutions including $BaTiO_3$, PZT, PLZT, PbN_2O_6, $NaNbO_3$, and PT. Foremost of these has been $BaTiO_3$, which dates from the early 1940s, but, in the past several decades, it largely has been supplanted by the PZTs and PLZTs for transducer applications.[2,3,4] This is because PZT and PLZT compositions

1. possess higher electromechanical coupling coefficients than $BaTiO_3$
2. have higher Curie temperature (T_C) values, which permit higher temperatures of operation or higher temperatures of processing during the fabrication of devices
3. can be easily poled
4. possess a wide range of dielectric constants
5. are relatively easy to sinter at lower temperatures than $BaTiO_3$
6. form solid-solution compositions with many different constituents, thus allowing a wide range of achievable properties.

PZT ceramics are almost always used with a dopant, a modifier, or other chemical constituent to improve and optimize their basic properties for specific applications.[5,6,7] Examples of these additives include off-valent *donors*, such as Nb^{5+} replacing Zr^{4+} or La^{3+} replacing Pb^{2+} to counteract the natural *p*-type conductivity of the PZT and, thus, increase the electrical resistivity of the materials by at least 3 orders of magnitude. The donors are usually compensated by A-site vacancies. These additives (and vacancies) enhance domain reorientation; ceramics produced with these additives are characterized by square hysteresis loops, low coercive fields, high remnant polarization, high dielectric constants, maximum coupling factors, higher dielectric loss, high mechanical compliance and reduced aging.[8]

Off-valent *acceptors*, such as Fe^{3+} replacing Zr^{4+} or Ti^{4+}, are compensated by oxygen vacancies and usually have only limited solubility in the lattice. Domain reorientation is limited, and, hence, ceramics with acceptor additives are characterized by poorly developed hysteresis loops, lower dielectric constants, low dielectric losses, low compliances, and higher aging rates. *Isovalent* additives, such as Ba^{2+} or Sr^{2+} replacing Pb^{2+} or Sn^{4+} replacing Zr^{4+} or Ti^{4+}, in which the substituting ion is of the same valency and approximately the same size as the replaced ion, usually produce inhibited domain reorientation and poorly developed hysteresis loops. Other properties include lower dielectric loss, low compliance, and higher aging rates.[8] The effects of all the dopants are summarized in table 1.1.

The piezoelectric activity in PZT solid solutions is optimum for compositions near the

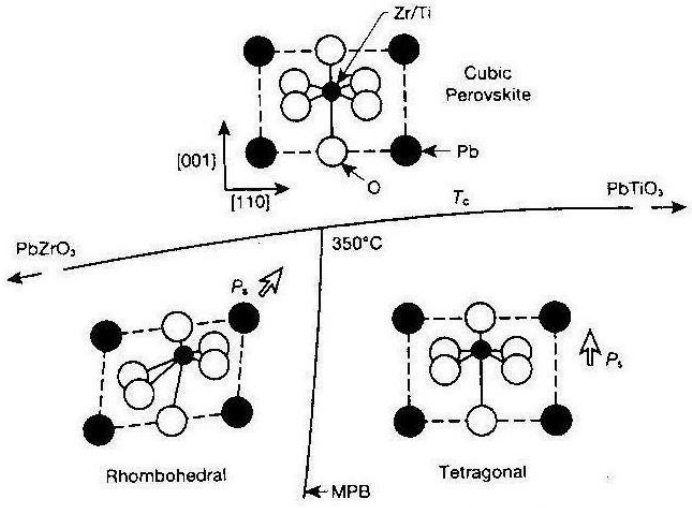

Figure. 1.1 Representing MPB between tetragonal and rhombohedral phases.

Morphotropic Phase Boundary (MPB). The MPB is almost a temperature independent phase boundary that separates two ferroelectric phases: a tetragonal crystal (P4*mm*) and a rhombohedral structure (R3c) as shown in Fig. 1.1. Compositions near the MPB may have both of these coexisting to give a total of fourteen possible polarization

directions (six tetragonal <001> and eight rhombohrdral <111> in reference to cubic prototype cell axes).

Table 1.1 Substitution Effects on Dielectric and Piezoelectric Properties.[1]

Property	Isovalent substitution	Acceptor Substitution	Donor Substitution
Curie Temperature	Lower	Higher	Lower
Dielectric Constant	Higher	Lower	Higher
Dielectric Loss	Lower	Lower	Higher
Electrical resistivity		Lower	Higher
Coercive force		Higher	Lower
Remnant Polarization		Lower	Higher
Piezoelectric Coefficient		Lower	Higher
Aging	Higher	Lower	Lower
Coupling Coefficient		Lower	Higher
Mechanical quality factor		Higher	Lower
Elastic Compliance	Lower	Lower	Higher
Strain hysteresis		Lower	Higher
Hysteresis squareness	Lower	Lower	Higher

The large number of polarization directions enables optimized crystallographic orientations to be established from grain to grain in the poling process, in turn, results anomalously high piezoelectric properties.

Further improvements in some of the piezoelectric properties are achieved through off valence and isovalence substitutions. The effects are described in table 1. Present work focuses on processing and piezoelectric properties in 9% Sr doped PZTs. Strontium is an isovalent substituent. The effects of Sr substitution in PZT have been studied by researchers and conclusions of their studies are as follows.

1. Sr substitution lowers the Curie point (Tc) which enhances the permittivity and also results in enhancement of d_{33}.[9] For every 1 atomic % addition there is 9°C decrease in Curie point. In Nb doped PZT ceramics, Sr. substitution up to 32 mol% decreases Tc from 360 to 30°C.[10] In addition to decreasing Tc, strontium broadens the phase transition maximum implying that the distribution of Curie temperature is increased.
2. Sr doping in PZTs promotes the tetragonal over the rhombohedral phase for a fixed Zr: Ti ratio.
3. The Sr substitution makes the domain width finer and distribution of domain widths is inhomogeneous even within a grain varying from 100 to 20 nm. This has the effect of increase in width of relative permittivity maximum.
4. Sintering of Sr substituted (12 mole %) PZTs above 1120 °C cause surface decomposition due to PbO loss at the surface. Consequently monoclinic ZrO_2 (second phase) forms which decreases maximum permittivity.[11]
5. Sr-doping produces hard type ceramics which are not easily depolarized.[12]

PZT compositions with 6 mole % Sr has been studied extensively[2,13-14] but compositions with higher Sr concentrations are rarely worked out. Previous works[15,16] discuss the effects of heating rate on the properties of PZT with 9 mole % Sr doping. Fast firing approach produces density of 7.66 g/cm^3 as compared to 7.40 g/cm^3 for conventional sintering which result in 30% greater mechanical strength and 7% greater charge coefficient (d_{33}).[15] According to the work by C-C-Hsueh et al[16] fast firing has the advantage of getting high dense ceramics with small grain size microstructure. Large grain sizes exhibit high dielectric constant, but incorporates high dielectric losses, so the firing process must be tailored to produce dense samples with suitable grain sizes for specific applications.

A systematic study in manufacturing of PZTs with higher Sr concentration (>6%) prepared from conventional mixed oxide route is still lacking. The purpose of present work is to assess the influence of higher Sr doping on dielectric and piezoelectric properties in PZTs and examine the changes occurring in microstructure and homogeneity as the manufacturing process proceeds from initial stage of mixing to final stage of sintering. To ascertain the total change occurred in properties by ageing, the sintered and poled samples were subjected to accelerated ageing by heating to 100°C for three days.

2 Dielectric and Piezoelectric Quantities

Lead Zirconate Titinates (PZTs) are basically dielectric materials. A dielectric material is one that is electrically insulating (nonmetallic) and exhibits or may be made to exhibit an electric dipole structure: that is there is separation of positive and negative electrically charged entities on a molecular or atomic level. All dielectric materials are good insulators but the converse is by no means true.[17] Dielectric materials can be divided into two parts depending upon its polarity: that is, polar and non polar. In polar dielectrics normally the dipoles are all randomly oriented, so the net dipole moment and hence the polarization of the dielectric is zero. When the material is subjected to an external electric field, the dipole moments tend to orient themselves in the direction of applied electric field. This results in a finite polarization. The polarization increases linearly with the applied electric field. When the electric field is removed the polarization becomes zero, because the dipole moments go back to random orientation configuration. In certain special type of polar dielectrics, the permanent dipole in the material are all oriented in a specific direction, even in the absence of an external electric field. These dipolar dielectrics are called ferroelectrics. The term 'ferro' originates from the fact that they are the dielectric analogue of ferromagnetic material, which may display permanent magnetic behavior. In ferroelectrics, there must exist permanent electric dipole. Ferroelectric materials are characterized by following special properties.

Ferroelectric hysteresis,

Spontaneous polarization,
Reversibility of polarization and
Ferroelectric transition temperature.

When a dielectric material is subjected to an electric field, the material gets polarized due to shifting of electron charge cloud (electronic polarization), shifting of positive and negative ions (ionic polarization) and due to orientation of dipoles (orientation polarization). When there is shifting of ions or change in orientation of dipoles there will be a slight change in the dimension of material. That is, application of electric field causes strain in dielectric which is independent of direction of dielectric. This effect exists in all dielectrics and is called electrostriction effect. In those dielectrics which have no center of symmetry, the strain produced due to application of electric field is directly proportional to applied field E; i.e. if the electric field is reversed to reverse the dipoles, the strain also changes sign (i.e. expansion becomes contraction and vice versa). Such dielectrics exhibit an additional effect, that is, when mechanical stress is applied to the material, the material gets polarized. Such materials are called piezoelectric materials. All ferroelectric materials exhibit piezoelectric effect because ferroelectric materials lack center of symmetry. Ferroelectric materials are a special class piezoelectric material because they exhibit certain other special characteristics mentioned earlier, in addition to exhibiting piezoelectric effect. Brief introduction to the properties most commonly used in evaluating the material is as follows.

2.1 Dielectric Constant

Consider a simple parallel plate capacitor with metal plates of area A separated by distance d, as shown in Fig. 2.1. Consider first the case in which the space between the plates is a vacuum. If a voltage V is applied across the plates, one plate will

acquire a net charge of +q and the other a net charge of –q. The charge q is found to be directly proportional to the applied voltage V as

$$q = CV \qquad \text{Or} \qquad C = q/V$$

where C is proportionality constant called the capacitance of the capacitor. The SI unit of capacitance is coulombs per volt (C/V), or the farad (F). Thus

$$1 \text{ farad} = \frac{1\ coulomb}{volt}$$

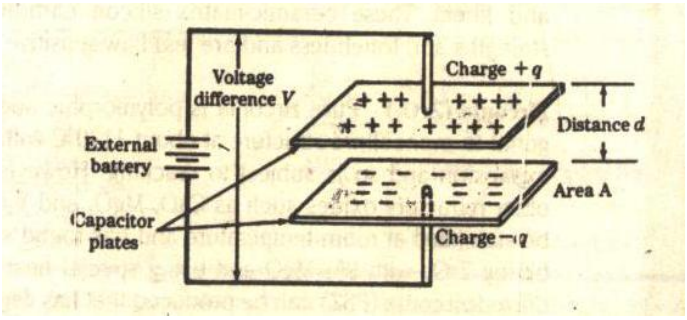

Parallel **Figure 2.1** plate capacitor.

Since the farad is a much larger unit of capacitance than is normally encountered in electrical circuitry, the commonly used unit are the picofarad (1 Pf = 10^{-12} F) and the microfarad (1 μF = 10^{-6}). The capacitance of a capacitor is a measure of its ability to store electric charge. The more charge stored at upper and lower plates of a capacitor, the higher is its capacitance. The capacitance C for a parallel plate capacitor whose area dimensions (A) are much greater than the separation distance (d) of the plate is given by

$$\mathbf{C = \epsilon_0 A/d} \qquad \mathbf{(2.1)}$$

where ϵ_0 = permittivity of free space = 8.854×10^{-12} F/m

When a dielectric (electrical insulator) fills the space between the plates (Fig. 2.2), the capacitance of the capacitor is increased by a factor **K**, which is called the dielectric

constant of the dielectric material. For a parallel plate capacitor with a dielectric between the capacitor plates,

$$C = K \in_0 A/d \qquad (2.2)$$

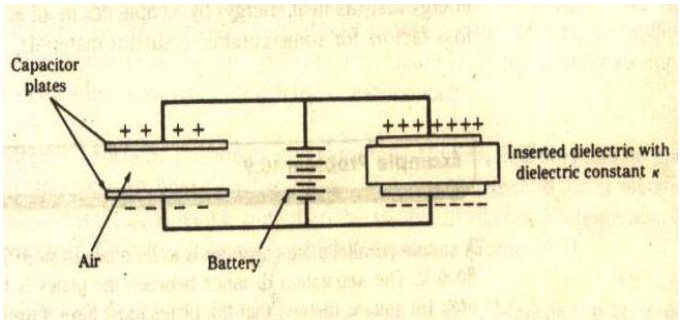

Figure 2.2 Parallel plate capacitor with dielectric material.

The energy stored in a capacitor of given volume at a given voltage is increased by the factor of the dielectric constant when the dielectric material is present. By using a material with a very high dielectric constant, very small capacitors with high capacitance can be produced.[18]

2.2 Dielectric Strength

Another property besides the dielectric constant that is important in evaluating dielectrics is the dielectric strength. This quantity is a measure of the ability of the material to hold energy at high voltages. Dielectric strength is defined as the voltage per unit length (electric field or voltage gradient) at which failure occurs and thus is the maximum electric field that the dielectric can maintain without electrical breakdown.

Dielectric strength is most commonly measured in volts per mil (1 mil = 0.001 in) or kilovolts per millimeter. If the dielectric is subjected to a voltage gradient that is too intense, the strain of the electrons or ions in trying to pass through the dielectric

may exceed its dielectric strength. If the dielectric strength is exceeded, the dielectric material begins to break down and the passage of current (electrons) occurs.[18]

2.3 Dielectric loss factor

If the voltage used to maintain the charge on a capacitor is sinusoidal, as generated by an alternating current, the current leads the voltage by 90° when a loss-free dielectric is between the plates of a capacitor. However, when a real dielectric is used in the capacitor, the current leads the voltage by 90°- δ, where the angle δ is called the dielectric loss angle. The product of K tan δ is designated the loss factor and is measure of the electric energy lost (as heat energy) by a capacitor in an ac circuit. Current voltage relationship is shown in Fig. 2.3.

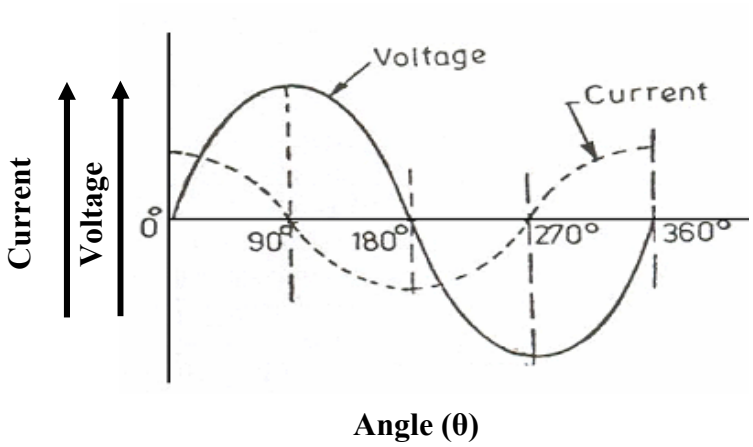

Figure 2.3 Current -Voltage relationship with angle (θ)

2.4 Piezoelectric Properties

2.4.1 Charge Constant (d)

Two effects are operative in piezoelectric crystals, in general, and in ferroelectric ceramics, in particular. The direct effect (designated as a generator) is identified with the phenomenon whereby electrical charge (polarization) is generated from a mechanical stress, whereas the converse effect (designated as a motor) is associated

with the mechanical movement generated by the application of an electrical field. Both of these effects are illustrated in Fig. 2.4 as cartoons for easy grasp of the principles. The basic equations that describe these two effects in regard to electric and elastic properties are

$$D = dE + \varepsilon^T E \qquad \text{(generator)} \qquad (2.3)$$

$$S = s^E T + dE \qquad \text{(motor)} \qquad (2.4)$$

where D is the dielectric displacement (consider it equal to polarization), T the stress, E the electric field, S the strain, d a piezoelectric coefficient, s the material compliance (inverse of modulus of elasticity), and ε the dielectric constant (permittivity). The superscripts indicate a quantity held constant: in the case of ε^T, the stress is held constant, which means that the piezoelectric element is mechanically unconstrained, and, in the case of s^E, the electric field is held constant, which means the electrodes on the element are shorted together. Equations (2.3) and (2.4), in matrix form, actually describe a set of equations that relate these properties along different orientations of the material. Because of the detailed nature of the many equations involved, the reader is referred to sources on the subject.[2,17] Suffice it to say that, because this is a piezoelectric solid, equations. (2.3) and (2.4) relate given properties,

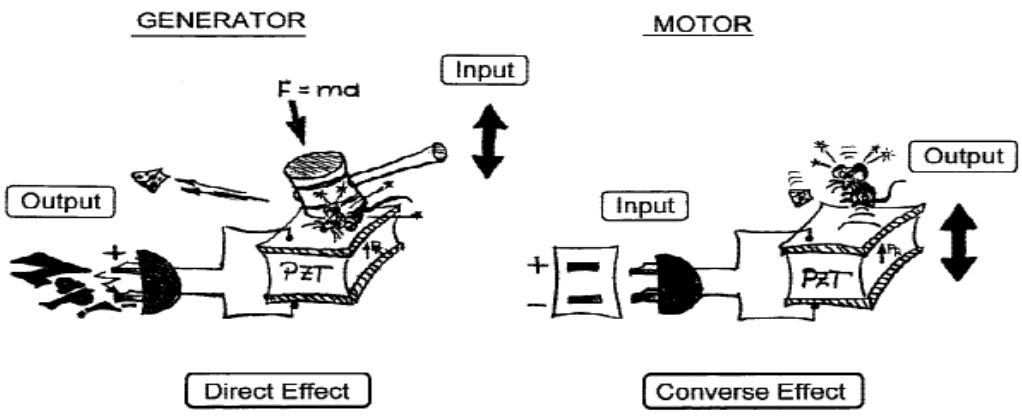

Figure 2.4 Direct and Converse Piezoelectric Effects.

such as electric displacement (polarization) and strain to both the mechanical and electrical states of the material. Furthermore, these properties are directional quantities, and, hence, they are usually specified with subscripts to identify the conditions under which they are determined, e.g., d_{31} indicates that this piezoelectric coefficient relates to the generation of polarization (direct effect) in the electrodes perpendicular to the 3 or vertical direction and to the stress mechanically applied in the 1 or lateral direction; d_{33} indicates the polarization generated in the 3 direction when the stress is applied in the 3 direction as shown in the Fig. 2.5**.**

Typical relationships for this coefficient are:

$$D_3 = d_{33}T_3 \text{ (direct effect)} \quad (2.5)$$

$$S_3 = d_{33}E_3 \text{ (converse effect)} \quad (2.6)$$

where d coefficients are numerically equal in both equations. The d coefficients are usually expressed as $\times 10^{-12}$ C/N for the direct effect and $\times 10^{-12}$ m/V for the converse effect. High d coefficients are desirable for those materials that are utilized in motional or vibrational devices, such as sonar and sounders.

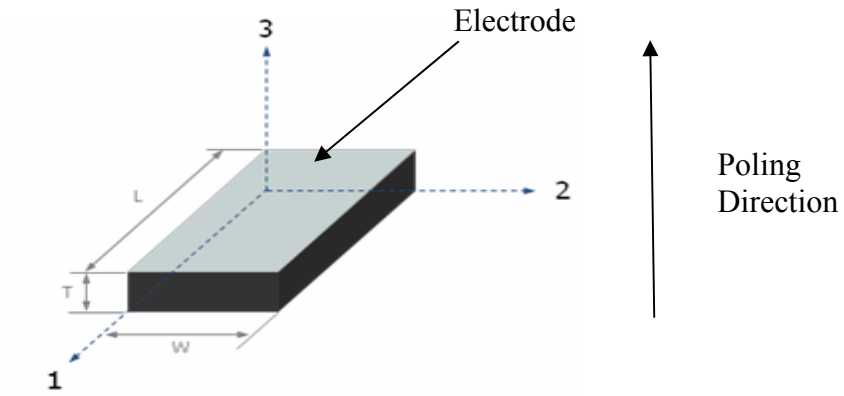

Figure 2.5 Nomenclature for designation of directional properties.

2.4.2 Voltage Constant (g)

In addition to the d coefficients, open-circuit g coefficients are also used to evaluate piezoelectric ceramics for their ability to generate large amounts of voltage per unit of input stress. The g constant is related to the d constant via the relationship

$$g = d / K \in_0 \quad (2.7)$$

where K is the relative dielectric constant and $\in_0$ the permittivity of free space (8.854×10^{-12} F/m). Thus, a high g constant is possible for a given d coefficient if the material has a low K. High-*g*-constant ceramics are usually ferroelectrically hard materials that do not switch their polarization readily and possess lower K values. They are used in devices such as portable gas igniters and patio lighters.

2.4.3 Piezoelectric Coupling Factor (k)

The piezoelectric coupling factor (e.g., k_{33}, k_{31}, and kp) is a convenient and direct measurement of the overall strength of the electromechanical effect, i.e., the ability of the ceramic transducer to convert one form of energy to another. It is defined as the square root of the ratio of energy output in electrical form to the total mechanical energy input (direct effect), or the square root of the ratio of the energy available in mechanical form to the total electrical energy input (converse effect). Because the conversion of electrical to mechanical energy (or vice versa) is always incomplete, k is always less than unity. Commonly used as a figure-of-merit for piezoelectrics, the higher k values are most desirable and constantly sought after in new materials. For ceramics, kp is a typical measurement used in comparing materials, ranging from 0.35 for $BaTiO_3$ to as high as 0.72 for PLZT. It can be represented in mathematical form as

$$k = \sqrt{\frac{\text{Mechanical Energy stored}}{\text{Electrical Energy Applied}}} \qquad \text{Indirect Effect}$$

$$k = \sqrt{\frac{\text{Electrical Energy Stored}}{\text{Mechanical Energy Applied}}} \qquad \text{Direct Effect}$$

Coupling coefficient (k) is determined by an instrument called Transducer Analyzer by applying the following formulae

$$k = \sqrt{\frac{F_a^2 - F_r^2}{F_a^2}}$$

Resonance frequency (F_r) is a condition in which a vibrating system responds with maximum amplitude to an alternating driving force. This condition exists when the frequency of the driving force coincides with the natural un-damped oscillatory frequency of the system Anti-resonance frequency (F_a) is a condition in which a vibrating system responds with minimum amplitude to an alternating driving force by virtue of the inertia and elastic constants of the system. Corresponding values for F_r and F_a are shown in the Fig. 2.6 (a) when the sintered and poled pellet was tested for measurement of coupling coefficient (k) in present study.

2.4.4 Mechanical Quality Factor (Q_M)

It is the ratio of reactance to resistance in the equivalent series circuit, representing the mechanical vibrating resonant systems or in another way it is ratio of strain in phase to strain out of phase with stress which becomes observable electrically through the piezoelectric effect. It is measured by a device called Transducer Analyzer by applying the following formulae

$$Q_M = \frac{F_r}{F_2 - F_1}$$

Where F_r is resonant frequency and F_2 and F_1 are frequencies for maximum and minimum susceptance (jB) when the device under test is passed through a frequency range. These frequencies are shown in the Fig. 2.5 (b). Mechanical quality factor Q_M is different from electrical quality factor (Q_E) found in dielectric literature. Q_E is inverse of tan δ.

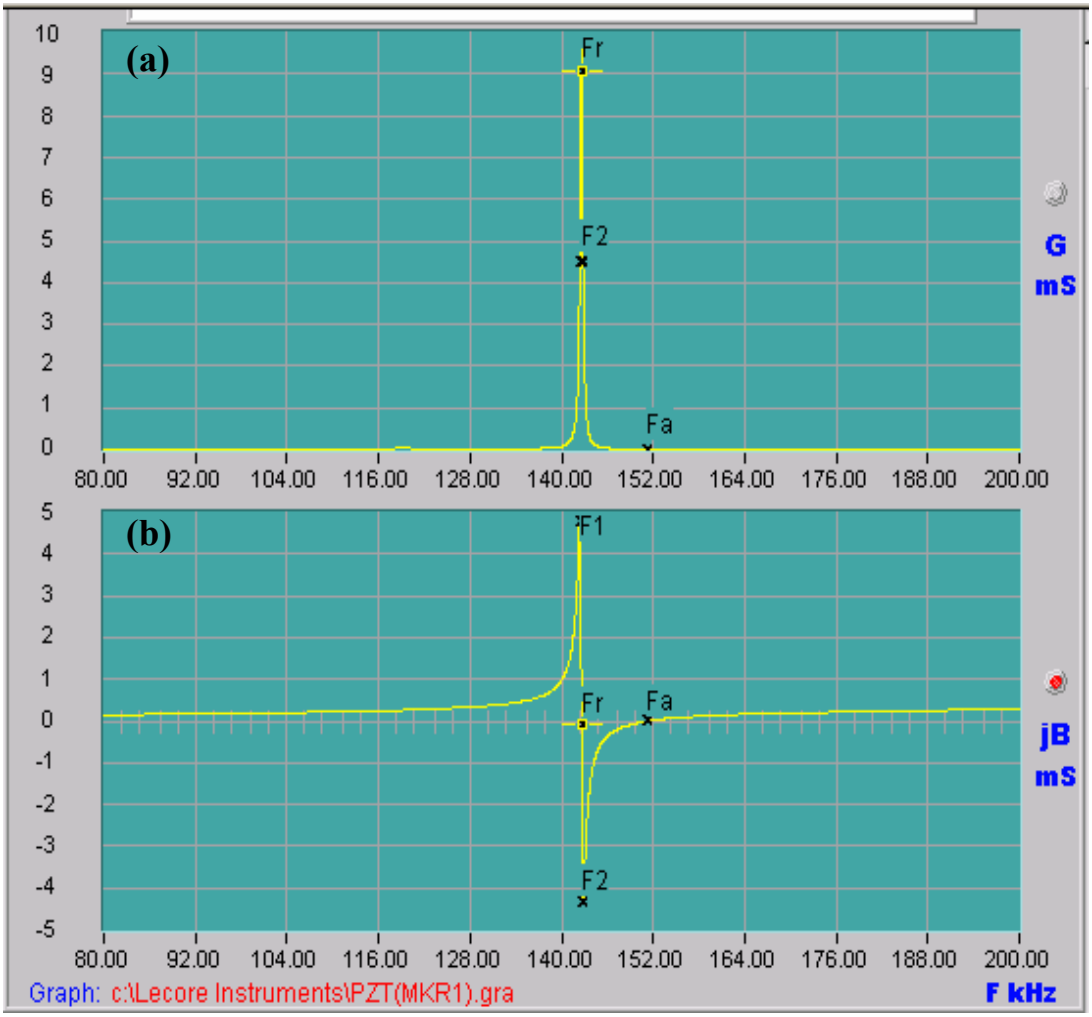

Figure 2.5 (a) Relationship between frequency (F) and conductance (G) and (b) relationship between frequency (F) and susceptance (jB).

3 Theory, Practice and Applications

In this section the basic theory of piezoelectricity, mechanism of obtaining high piezoelectric properties and process variables that influence the final properties as well as some applications will be presented.

3.1 Perovskite Structure

Ceramic materials including PZT which exhibits piezoelectricity have perovskite structure. The generalized perovskite structure ABO_3 is visualized as cubic close packing assembly (Fig. 3.1) of composition AO_3 with the A ion coordinated with 12 oxygen ions and B ion in the octahedral interstices. While no one sub lattice is actually close packed, the structure can be considered an FCC-derivative structure in which the larger A cation and oxygen together form an FCC lattice. The smaller B cation occupies the octahedral sites in this FCC array and has only oxygen as its nearest neighbors.[19] The ions that lie at the corners of the unit cell are termed as A site and in PZT it is occupied by Pb^{+2} ions and the ion which lie at interstices in oxygen octahedra are called B site. Zr or Ti ion fills this space in PZT. The arrangement of cations and anions is such that cations are shielded from one another by oxygen ions. Each oxygen ion (in face position in unit cell) is coordinated by four Pb (at the corners of unit cell) and two Ti or Zr ion. The oxygen octahedral only share corners with each other but they unavoidably share faces with 12-fold Pb polyhedra (dodecahedra). Interstitial space in oxygen octahedra is larger than the size of B

cation so that it can rattle around in the space and may go close to any oxygen ion when acquire stable position. A most important feature of this spontaneous displacement is that it results in a permanent electrical dipole. In PZT a lot of variation in properties are achieved by replacing ions at A and B site by isovalent and aliovalent substitutions.[2, 8, 17, 20, 21]

When PZT ceramic is cooled from higher temperature, phase changes do occur. Above the Curie point (approximately 380 °C) the unit cell is cubic with the ions arranged in a pattern as shown in the Fig. 3.1. Below the Curie point (Tc) the structure is slightly distorted to the tetragonal form with a dipole moment along the c direction for Ti rich compositions and to Rhombohedral form with a dipole moment along

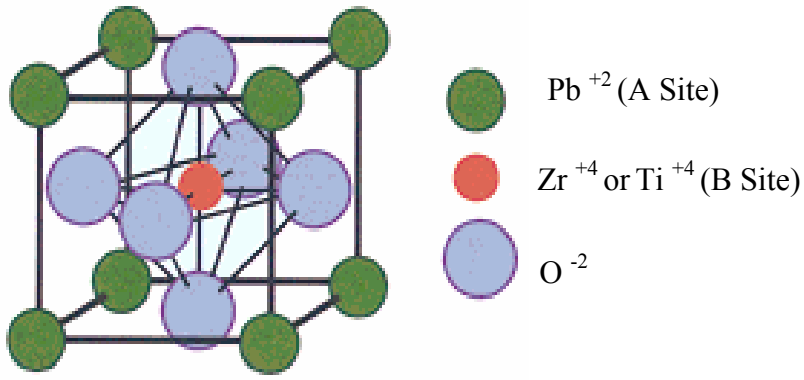

Figure 3.1 Unit Cell for Perovskite Structure.

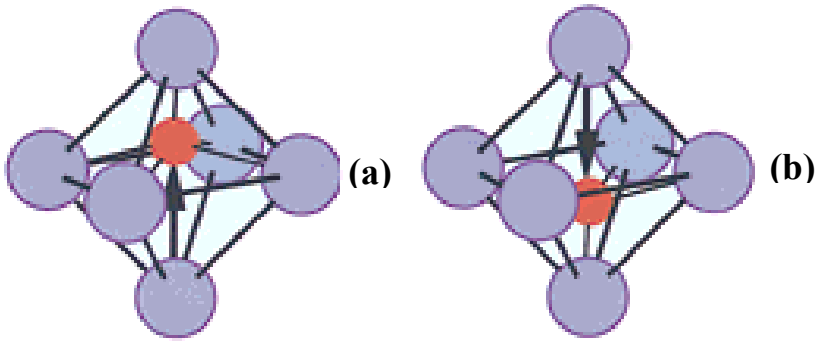

Figure 3.2 Polarization due to displacement of B site cation (a) Polarization Up (b) Polarization Down.

body diagonal for Zr rich compositions. Shifting of B site ion in upward and downward directions is shown in the Fig. 3.2 giving rise to upward and downward polarization due to formation of dipoles.

3.2 Domains and Polarization

The spontaneous alignment of dipoles over many unit cells results in formation of a micro structural entity known as ferroelectric domain. For example, when the cubic paraelectric phase in $BaTiO_3$ transform to tetragonal phase upon cooling below Curie point, the displacement of the Ti^{4+} ion can occur along one of the six <100> directions of the cubic phase. A cooperative alignment among neighboring unit cells results in the formation of a ferroelectric domain which must be oriented in any one of these six directions. If only one orientation to form throughout a single crystal, then we have a single domain, and the opposing surfaces of the crystal where the polarization terminates would be oppositely charged as shown in the Fig. 3.3(a). This kind of long range charge separation is energetically unfavorable and instead a number of domain orientations tend to form in all but the smallest crystallites, resulting in a net zero macroscopic polarization as illustrated in Fig. 3.3(b).

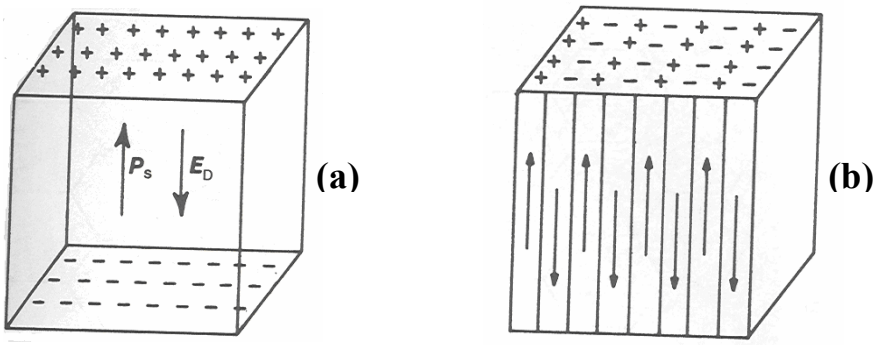

Figure 3.3 (a) Surface charge associated with spontaneous polarization (b) formation of 180° domains to minimize electrostatic energy.

In tetragonal $BaTiO_3$ and PZT adjacent domains can have their polarization vectors in antiparallel directions or at right angles to each other. The boundaries between these domains are, correspondingly, known as 180° or 90° domain walls. These domains and corresponding domain walls are shown in the Fig.3.4. Domain walls are about one unit cell in thickness (varies with temperature and crystal purity) and have a small positive energy (2-4 ergs/cm^2 for 90° walls, 7-10 ergs/cm^2 for 180° walls). The formation of ferroelectric domains to avoid long range charge separation comes at the expense of this interfacial energy. The domain structure revealed by polishing and

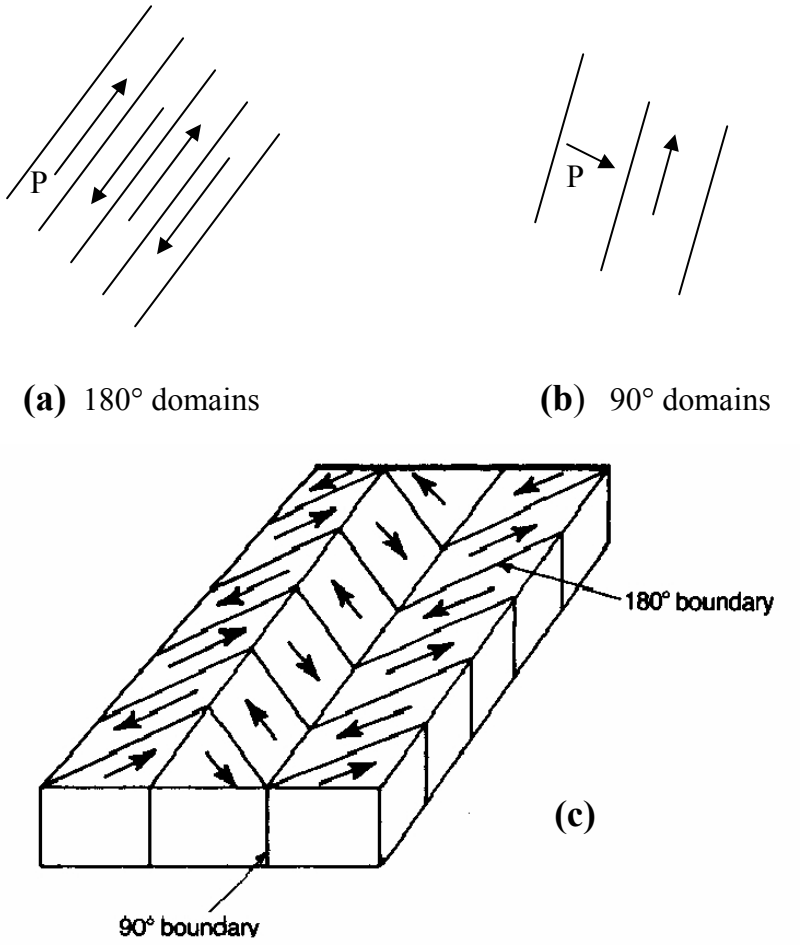

Figure 3.4 (a) 180° domains (b) 90° domains (c) boundary between 180° and 90° domains.

etching in an unpoled ceramic in shown in the Fig. 3.5. The principle features in the form of parallel lines are due to 90° changes in polar direction.

Figure 3.5 Polished and etched surface of unpoled ceramic.

3.3 Poling

One of the most valuable features of ferroelectric ceramics is that they can be transformed into polar material by applying a static field. This process is called poling. The process is carried out by applying electric field (1-4 KV/mm) across the ceramic body at temperature 100-150 °C. A polycrystalline ceramic that has not been subjected to static electric field behaves as non polar material even though crystals comprising it are polar. The process of poling is illustrated in the Fig. 3.6. Fig. 3.6 (a) shows the structure of grains before application of field. Each grain is non polar because of cancellation of both 180° and 90° domains. Fig. 3.6 (b) shows grains structure after applying electric field, the 180° domains switch. This switching is due to movement of B site ions (Ti^{4+} or Zr^{4+}) in reverse direction of the polarity at that point. When this happens the energy barriers for neighboring ions are reduced and the entire region affected by the field will eventually switch into the new direction. The

switching of 180° domains will produce net overall polarity but no dimensional change. With increase in electric field 90° domains will switch accompanied by small elongation, Fig. 3.6 (c). Elongation occur due to the fact that polar ***c*** axis is longer than non polar ***a*** axis. Due to this elongation switching is difficult in these domains and takes place at higher fields.

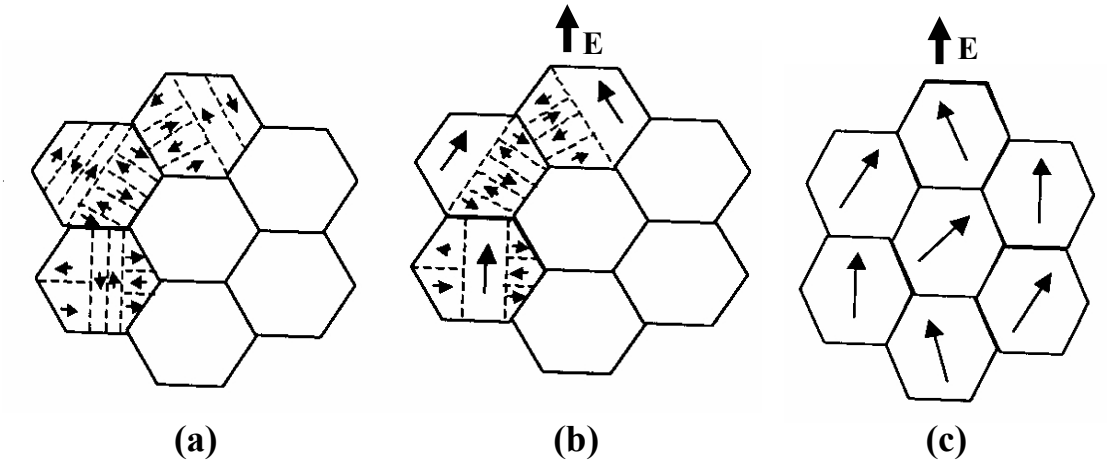

Figure 3.6 Changes accompanying application of electric field (a) the structure of grains before application of static electric field (b) with applied electric field- 180° domain switch (c) with increase in electric field both 180° and 90° domains switch.

The random directions of the crystallographic axes of the crystallites of a ceramic limit the extent to which spontaneous polarization can be developed. It has been calculated that the fraction of single crystal polarization value that can be obtained in ceramics in which polar axis take all possible alignments are 0.83 and 0.87 for perovskites with tetragonal and rhombohedral structures respectively. In ceramic tetragonal $BaTiO_3$ the saturation polarization is about half the single crystal value. The value attainable is limited by the inhibition of 90° switching because of the strains involved although 180° switching is complete.

3.4 Domain Wall Mobility

Piezoelectric properties in ferroelectric ceramics are greatly affected by domain wall mobility. Conditions that will enhance domain wall mobility will increase the piezoelectric coefficients and the conditions that inhibit the mobility will diminish the piezoelectric coefficients. The piezoelectric coefficients are maximum at Morphotropic Phase Boundary (MPB) but they are also influenced by dopants and defect structures because of their influence on domain wall motion.[22] Donor doping is not effective at pinning the domain walls. Pinning is believed to result from the defect dipoles aligning with the polarization in the domain which occurs as the temperature falls below the Curie temperature where diffusion rates are slow. For PZT this is Tc = 350°C. When the dopant Nb^{+5} is substituted for Ti $^{4+}$, vacancies occur in the Pb sites. In this soft (Nb^{+5}) PZT the domain wall movement contributes to the size of the dielectric and piezoelectric coefficients and so they are used as hydrophones and ultrasonic detectors where high sensitivity is required. However soft PZT are easily depoled because the domain walls are not pinned hence soft PZT is not used for transmitters.

Acceptor doping with K^{+1} substituting for Pb^{+2} or Fe^{+3} for Ti^{+4} is used to make “hard” PZT. This doping produces pinned domain walls because the defect dipoles are able to align with the domain structure. Dipoles which are oxygen vacancies and associated dopant ions are more easily able to re-orientate in “hard” PZT because oxygen vacancies are able to diffuse at the temperature below Tc. In the perovskite structure oxygen sites are adjacent to each other, therefore, oxygen can easily move into oxygen vacancies realigning defect dipoles and pinning domain walls.

3.5 Ageing

For perovskite ceramics such as $BaTiO_3$ and $Pb(Zr,Ti)O_3$, the domains are unique and intrinsic micro structural features, and they are fundamentally associated with the ferroelectric properties of the materials. On the other hand, it is well known that the various properties of these materials are time dependent, which is usually referred to as aging. Even in the absence of an external electric or stress field, the dielectric constant decreases and other ferroelectric properties change with time.[23] Different mechanisms have been suggested to explain the aging phenomenon. Bradt *et al*[24] have proposed that aging is related to the relief of residual stresses of the ferroelectric transition and the consequent change in the domain structure. Ordering of defects inside the domains,[25] segregation of defects on the domain walls[26] and reorientation of dipolar defects[27] have also been proposed to be the causes of aging. Although the nature and contribution of each mechanism to ageing is not precisely known, in any case, aging has been predicted to involve the stabilization of domain structures.[28]

3.6 Fabrication of PZT

Normal powder technology is used in the fabrication of PZT ceramics. The highest values of coefficients are obtained when the composition is near the stoichiometric, the contents of impurities are minimal and the density is as high as possible.

To achieve these objectives both solid oxides and chemical method can be employed but PZT ceramics continue to be prepared from the most economical, mixed-oxide (MO) process[29], although the demand for higher quality product emphasizing to adopt chemical methods. Contamination during milling is kept low by using ZrO_2 based milling media. [9,10,15,16,17,30,31,32] Most of the compositions used at present contain PbO as major constituent. Despite its volatility above 800°C the PbO must be retained

during sintering at temperatures up to 1300°C. A. I. Kingon and B Clark[33,34] address in some detail the matter of "atmosphere control" with regard to sintering PZT, and the effect of PbO content on densification kinetics. In his work[33,34] it is shown that excess PbO decrease the final density and the decrease in density is proportional to content of excess PbO added while 1.5 % PbO deficiency results in high density. A compositional fluctuation and compositional change in PZT ceramics was observed with excess PbO due to a difference of dissolution rate of TiO_2 in the PZT phase into the liquid PbO phase.[35] Calcination is usually carried out in lidded alumina pots [9,10,15,16,17]. For the final sintering the "work" is surrounded by a lead rich powder, such as $PbZrO_3$, and again placed in closed saggers. Because of the limited access to the atmosphere that results and the ease with which PbO is reduced to metallic lead, all organic constituents must be removed before sintering by a preliminary firing at about 600°C in air. The final firing is usually carried out in batch type electric kilns well filled with "work". Despite precautions, there is normally a loss of 2-3 % of the initial PbO content which is compensated by an addition to the starting materials.

An alternative to firing in closed vessels is very rapid firing in which the material, carried on a moving belt, is exposed to a high peak temperature for a brief time in a special kiln. This procedure is applicable to thin sheets of material.

Probably, a better alternative is to use a sintering aid so as to get the desired densification exploiting the liquid phase sintering at a lower temperature. However, the selection of sintering aid is crucial because they should not degrade the piezoelectric properties of PZT. So far, a lot of sintering aids have been tried by different workers with varying success. Some examples[36,37] of sintering aids are P_2O_5, Li_2CO_3, Na_2CO_3, B_2O_3, Bi_2O_3, V_2O_5, Cu_2O–PbO, etc. However, the incorporation of

such extraneous components in PZT degrades the d_{33} and g_{33} values in most of the cases.

A further difficulty with composition containing substantial amounts ZrO_2 results from the low reactivity of some grades of the material. The TiO_2 powders, developed as pigments, react rapidly with PbO, and the resulting titanates only take up Zr^{4+} ions slowly from unreacted ZrO_2[38]. Grades of ZrO_2 are available which have not been calcined at high temperatures during their preparation and which therefore react more rapidly with PbO so that a mixed $Pb(Zr,Ti)O_3$ is formed at an early stage. The problem can also be alleviated by prolonged milling in the mixing stage and by a second calcination after milling the product of an initial firing.

All the constituents of a PZT composition can be precipitated from nitrate solutions to yield highly homogenous reactive powders. Such powders can also be prepared by calcining citrates that contain the A- and B-site ions in a 1:1 ratio. It is possible to sinter at lower temperature using these materials and, apart from the economy in energy, this has the advantage of lessening the loss of PbO through volatilization. However, sintered bodies adequate for the majority of piezoelectric applications are obtained by the lower-cost route starting from a mixture of oxides and carbonates. Simple shapes are formed by die-pressing, long body of uniform section are formed by extrusion, thin plates are formed by band-casting or calendaring, and large rings and more intricate shapes are formed by slip-casting.

The sintered product usually has a density higher than the 95% of theoretical and a crystallite size in the 5-30 μm range. Both an excess and a deficiency of PbO result in inferior piezoelectric properties so that careful control of all aspects of the manufacturing process is essential.

Electrodes are applied after any necessary machining to shape or finishing. For the majority of applications a suitably formulated silver-bearing paint is fired on at 600-800°C. In the case of thin pieces, a Ni-Cr or gold electrodes can be applied by sputtering or evaporation.

Poling takes place with the specimens immersed in transformer oil at 100-150°C and with an applied field of 1-4 MV/m. In the case $BaTiO_3$ the field must be maintained whilst cooling to some 50°C below the Curie point. For PZT, the temperature and voltage are optimized to give the maximum piezoelectric coefficients without allowing the leakage current to reach levels that could result in thermal run away and electrical breakdown. Higher fields can be used if they are applied as a succession of shot pulses.

3.7 Precursor Powder Properties

Some physical and mechanical properties for precursor powders used in the fabrication of PZT are listed in Table 3.1. These properties are useful in evaluation of their contribution to different processing steps such as mixing, milling, calcination and sintering.

Table 3.1. Properties of precursor powders.

	PbO Litharge	**TiO_2 Anatase**	**ZrO_2 Monoclinic**	**$SrCO_3$**
Density gcm^3	9.64	3.89	5.68	3.50
Melting Point °C	886	1825	2700	1494
Hardness Mohs	02	5.5-6.0	9.5-9.8	3.50
Refractive Index	2.535	2.488	2.4	1.518

3.8 Applications

With the development and improvement of the lead zirconate - lead titanate ceramic materials (PZT) and components based on them, the number of applications grew very rapidly and continues to do so to this day. A comprehensive description of all applications is practically impossible. The following is intended only to outline the characteristic features of typical applications. Piezoelectric ceramic components are electromechanical transducers. They are able to convert mechanical forces from pressure, strain or acceleration into an electrical potential (direct piezo effect) and convert an electrical potential into mechanical motion (inverse piezo effect).

These effects open up a wide range of applications in all areas of engineering. Use is made both of converting electrical voltages into mechanical motion (piezoelectric actuators) or vibrations (sonic and ultrasonic transmitters), and of the conversion of mechanical forces and accelerations (sensors) or acoustic signals (sonic and ultrasonic receivers) into electrical signals. The ultrasonic signal processing, whether using the direct or inverse piezo effect, is based on the evaluation of propagation times, reflection and phase shift, etc. of ultrasonic waves. Operation is possible in a wide frequency range (a few Hz to a few MHz). Applications based on these two effects are given in table 3.2. A short description of some of applications is as follows.

3.8.1 Use in Hard Disc Drive

The recording density of magnetic hard disc drives (HDD) has been increasing with astonishing speed. The technical leap which allows much narrower data track width is expected. This requires high bandwidth servo position control of the read/write (R/W) head because the head must follow the narrow data track with high accuracy. A slider driven device, which including a pair of moonie piezoelectric (PZT) micro actuators

and a frame holder, is used to achieve more accurate positioning of the magnet head and to increase the servo bandwidth.[39]

Table 3.2 Applications of Piezoelectric Materials.

Use of Direct Piezoelectric Effect	**Use of Indirect Piezoelectric Effect**
Mechano-electrical	***Electro-mechanical***
Accelerometers	Actuators such as translators, bender elements and piezomotors
Igniters	Micro and Nano Positioning
Piezo Keyboards	Laser Tuning
Generators	Active Vibration Damping
Passive Damping	Micro Pumps
	Pneumatic valves
Acousto-electrical	***Electro-acoustical***
Acoustic and ultrasonic receivers	Signal generators (buzzers)
Noise Analysis	High voltage sources/transformers
Acoustic emission spectroscopy	Delay lines
	High power ultrasonic generators for cleaning, welding, aerosol production etc.
Use of both Effects	
Level measurement Flow rate measurement Object recognition Medical diagnostics High resolution material testing Sonar and echo sounders Adaptive structures	

3.8.2 Ultrasonic Imaging

Ultrasonic imaging in the frequency range from a few MHz to beyond 20 MHz has been used for diagnosis of many diseases. Ultrasound at frequencies higher than 20

MHz has applications in dermatology, ophthalmology and intravascular imaging. The performance of ultrasonic imaging systems especially at high frequencies depends critically upon the transducers/arrays, the design of which in turn is determined to a large degree by the materials and fabrication methodology of the piezoelectric element and supporting structures. The intra vascular catheter, used on a routine basis to image arterial tissue, is an essential medical tool enabling the surgeon to identify disease type and to take appropriate steps to combat it. A typical design is shown in the Fig. 3.7, which comprises an array of 64 PZT bars arranged around the catheter tip. Many development problems have been encountered and overcome, including the risk of depoling during processing (cutting, bonding, welding, sterilization) and of fractures due to stresses imposed on the elements during bending the array to conform to the catheter surface. Because both types of faults can degrade the image, the achievement of optimum mechanical strength is of the utmost importance demanding a very high quality microstructure free from any stress raising defects.

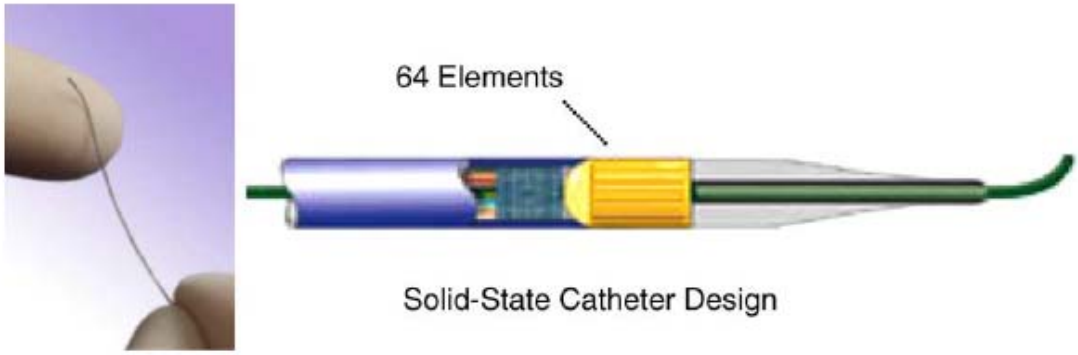

Figure 3.7. A typical design for a solid state catheter.

3.8.3 Wave Filters

Piezoelectric crystals, notably quartz, are used to control or limit the operating frequency of electrical circuits. A well known example is their use in quartz clocks.

The fact that a dielectric body vibrating at resonating frequency can absorb considerably more energy than at other frequencies provides the basis for piezoelectric wave filters. A filter is required to pass a certain selected frequency band, or to stop a given band. The pass band for a piezoelectric device is proportional to k^2 where k is appropriate coupling coefficient. Filters made on this principle from PZT ceramics have been widely used in the intermediate frequency stages of FM radio receivers. More stable units suitable for telecommunication filters are made from single crystal $LiTaO_3$.

3.8.4 Transformer

The transfer of energy from one set of electrodes to another on a piezoceramic body can be used for voltage transformation. In Fig. 3.8 a flat plate carries electrodes on half of its major surfaces and on an edge. The regions between larger electrodes, and between them and the edge electrode are poled separately. A low a.c. voltage is applied to the larger area electrodes at a frequency which excites a length mode resonance. A high voltage output can then be taken from small electrode and the common of the larger ones. The transformation can, very approximately, be in the ratio of the input to output capacitances but depends strongly on the output load, as does the efficiency. The ceramics needs to combine high k_{31} and k_{33} coupling coefficients with a high Q_m, preferably exceeding 1500. Very significant gains in voltages and amplification can be made by adopting a multilayered structure for primary and for both primary and secondary when the efficiency depends upon k^2_{33}.

In addition to suitability to cheap mass production, piezoelectric transformers offer the advantage of a low profile when mounted on printed circuit boards. Over recent years they have found a commercially significant application for powering fluorescent

lamps for back-lighting the screen in lap-top computers and electronic notebooks with liquid crystal displays.

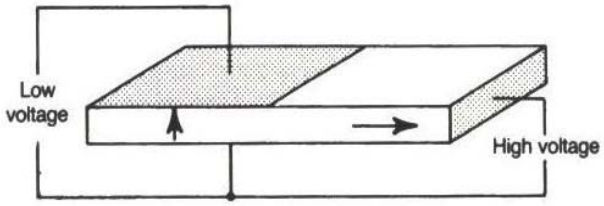

Figure 3.8 A simple form of piezoelectric transformer.

3.8.5 Stack actuator and '*Moonie*'

Multilayer stack actuators can be made in much the same way as a multilayer capacitor. However, because of the design of a MLCC each layer is clamped at its edges resulting in the development of electric field-induced mechanical stresses which can be a cause of eventual failure. In the case of the actuator the objective is to achieve maximum strain and if the same construction were applied as in the case of the MLCC dangerously large stresses would be developed which only would detract from the desired movement but would constitute a serious failure risk. The problem is avoided by extending the electrodes to the edge of each layer and devising a means of connecting up alternate layers without the risk of shorting to adjacent layers. This can be achieved in a variety of ways and one strategy is illustrated in Fig. 3.9. The attractive features of a piezoelectric/electrostrictive actuator are mentioned above, but a penalty is the small displacements generated. For a d_{33} value of 500pCN^{-1}(or, more appropriately in the present context, pmV^{-1}) a voltage of 1000 V applied across a 1mm thick poled disk would produce a displacement of only 0.5 μm. A multilayer stack of the same piezoceramic comprising 10 layers, each 100 μm thick, would produce a displacement of 5 μm for same applied voltage. Alternatively, the

multilayer stack allows low operating voltages for a given displacement. Various designs have been developed to magnify the small displacements, at the cost of reduced blocking force. A well known design, the Moonie, is illustrated in Fig. 3.10. The brass end-caps not only follow the d_{33}-controlled displacement but also redirect the d_{31} in displacement into the 3-direction. This magnified displacement can be as much as 20 μm on a 3mm thick actuator for an applied voltage of as little as 50 V.

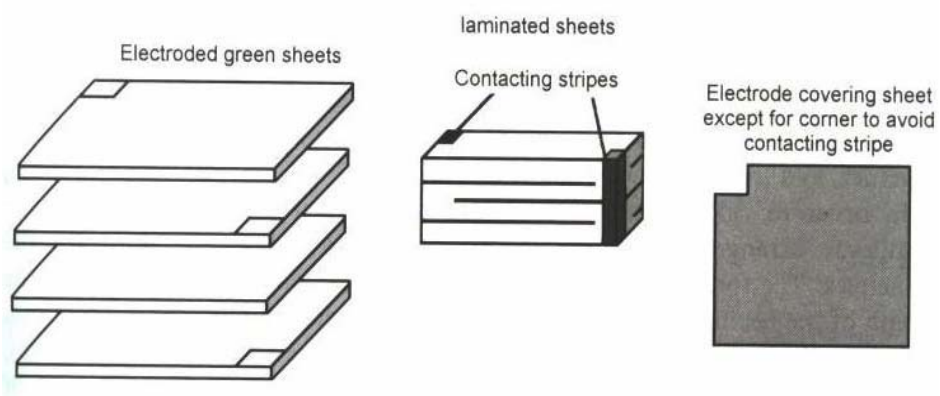

Figure 3.9. The multilayer stack actuator showing one strategy for electroding to avoid clamping stresses.

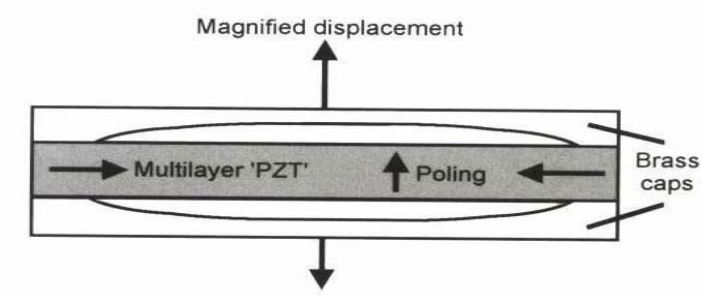

Figure 3.10. A Moonie Actuator.

4 Characterization Techniques and Equipments for Processing

A brief introduction to instruments used for measurement of dielectric and piezoelectric properties, and techniques of characterization and equipments used for processing are given in this section. These include LCR meter, d_{33} meter, Transducer Analyzer, SEM equipped with EDX, XRD, Planetary Mill and Particle Size Analyzer.

4.1 LCR meter

LCR (inductance-capacitance-resistance) meter is widely employed for measurement of capacitance, resistance, inductance and dielectric loss in PZT ceramics. A typical LCR meter is shown in the Fig. 4.1. Capacitance and dielectric loss (Tanδ) are measured by ac bridge circuits. The principle and circuit diagram for such a bridge (Schering Bridge) is explained in the following paragraph.

Scherring bridge is used for measurement of capacitance and dielectric loss of a capacitor.[40] In fact, it is a device for comparing an imperfect capacitor C_2 in terms of loss free standard capacitor C_1. The imperfect capacitor is represented by its equivalent loss free capacitor C_2 in series with a resistance 'r'. For high voltage applications, the voltage is applied at the junctions shown in the Fig. 4.2a. The junction between arm 3 and arm 4 is earthed. Since capacitor impedances at lower frequencies are much higher than resistances, most of the voltage will appear across capacitors. Grounding of the junctions affords safety to the operator from high voltage

hazards while making balancing adjustment in arm 3 arm 4. Now when the circuit is balanced it can be shown by applying cross multiplication rule that

$C_2 = C_1(R_4/R_3)$ and $r = R_3(C_4/C_1)$

Figure 4.1 A LCR meter used to measure dielectric properties.

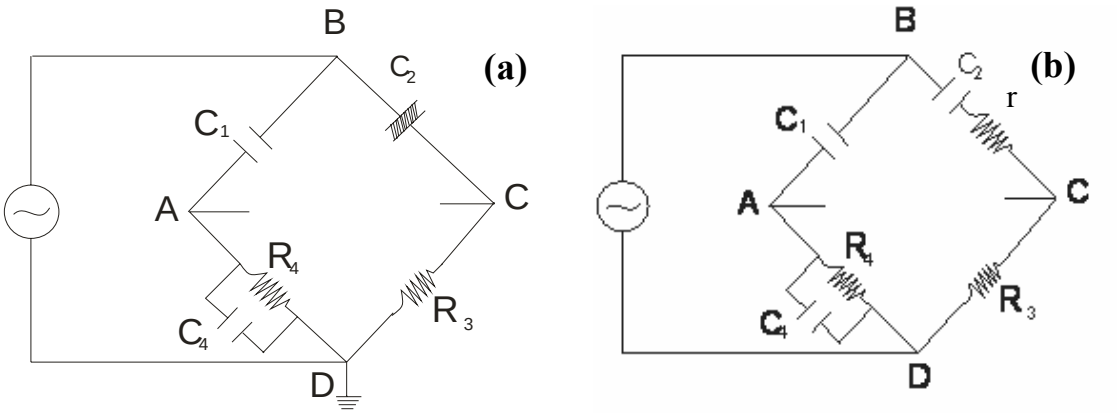

Figure 4.2. Circuit diagram for Sherring Bridge (a) Circuit for a perfect capacitor (b) Circuit for a imperfect capacitor.

The quality of a capacitor is usually expressed in terms of its phase defect angle or dielectric loss angle which is defined as the angle by which current departs from exact quadrature from the applied voltage i.e. the complement of the phase angle. If Φ is the actual phase angle and δ is the defect angle, then $\delta + \Phi = 90°$. For small value of δ, $\tan\delta = \sin\delta = \cos\Phi$ (approximately). Tanδ is usually called the dissipation factor of the

R-C circuit. For low power factors, therefore, dissipation factor is approximately equal to the power factor.

As shown in Fig. 4.3,

Dissipation factor = power factor = tan δ

$$= \frac{r}{Xc} = \frac{r}{1/\omega C_2} = \omega r C_2$$

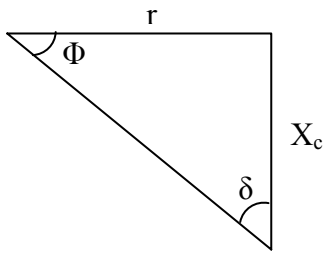

Fig. 4.3 Relation between resistance 'r' and reactance 'X_c'

Putting the value of the rC_2 from above,

Dissipation factor = $\omega r C_2 = \omega C_4 R_4$ = power factor.

4.2 d_{33} meter

The meter is used for the measurement of charge coefficient, d_{33}, which is the quantity of charge developed per unit force applied and is expressed in terms of pC/N. A typical d_{33} meter is shown in Fig. 4.4. Basic principal is that a device under test is clamped within the jaws of a force head unit and is subjected to oscillating force. The charge developed by the sample is measured. The force is applied by means of electromagnetic transducer. This force is preset to 0.25 N and is regulated by means of current control amplifier. The oscillator may be set to any frequency in the range of 30-300Hz. The test frequency is usually unimportant, unless the sample is a thin sheet or particularly massive. If this is the case a lower frequency may be used to avoid resonance problems.

4.3 Transducer Analyzer

Transducer Analyzer (shown in Fig. 4.5 a) is used to measure mechanical quality factor (Qm) and coupling coefficient (k) by measuring the resonant and anti resonant frequencies. The instrument works on the same principal as LCR meter with provision

Figure 4.4 A typical d_{33} meter employed to measure charge coefficient d_{33}.

of giving a selected range of frequencies automatically to device under test. A circle plot is drawn between conductance G and susceptance jB by varying the frequency in the given range. The formulas used for measurement of two parameters are as follows.

$$Q = \frac{F_r}{F_2 - F_1} \qquad k = \sqrt{\frac{F_a^2 - F_r^2}{F_a^2}}$$

Where F_r is resonant frequency, F_a is antiresonant frequency, F_1 is frequency for maximum B and F_2 is frequency for minimum B. The corresponding frequencies are shown in the Fig. 4.6 (a,b).

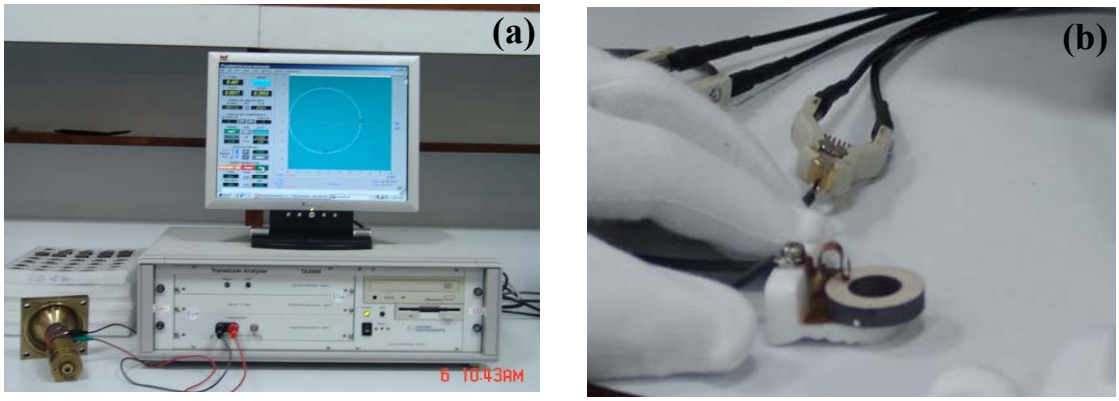

Figure 4.5. (a) Tranducer Analyzer (b) Test sample under test by Transducer Analyzer.

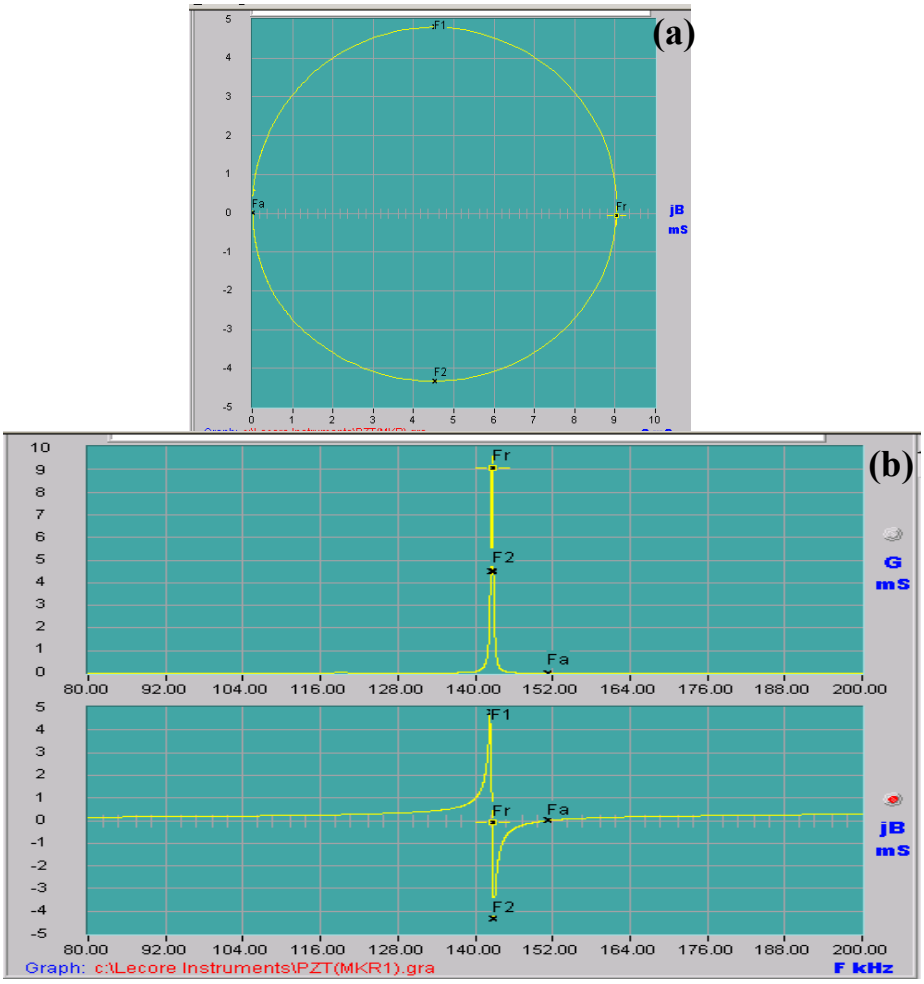

Figure 4.6. (a) A cicle plot drawn by Tranducer Analyzer (b) The circle plot splitted to show variation of conductance(G) and susceptance (jB) with frequency. Corresponding frequencies Fr, Fa, F_1 and F_2 for measurement of Qm and k are shown.

4.4 X- Ray Diffraction (XRD)

X-Ray Diffraction is a powerful technique used to uniquely identify the crystalline planes in materials and to measure the structural properties (strain state, grain size, phase composition, preferred orientation and defect structure) of these phases.

Here the fundamental principles of XRD technique are briefly discussed, the reader is referred to the work by Cullity[41] for more detail. Fig. 4.7 shows the basic features of an XRD experiment, where the diffraction angle 2θ is the angle between the incident and diffracted X -rays. In a typical experiment, the diffracted intensity is measured as a function of 2θ and the orientation of the specimen, which yields the diffraction

pattern, The X-ray wave length λ is typically 0.7-2 Å, which corresponds to X-ray energies (E= 12.4keV/ λ) of 6-17 KeV.[42]

Before considering the conditions for XRD, we will briefly review some important properties of crystalline materials. Crystals consists of planes of atoms that are spaced a distance d apart (Fig. 4.8 and Fig. 4.9), but can be resolved into many atomic planes, each with a different d-spacing.

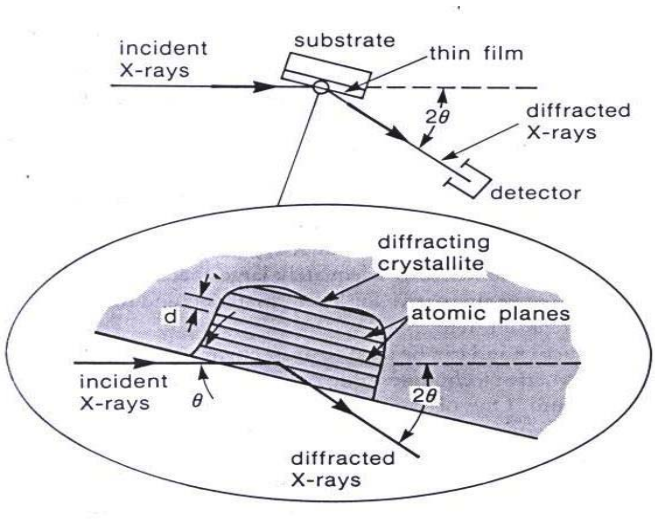

Figure 4.7 Basic features of XRD setup.

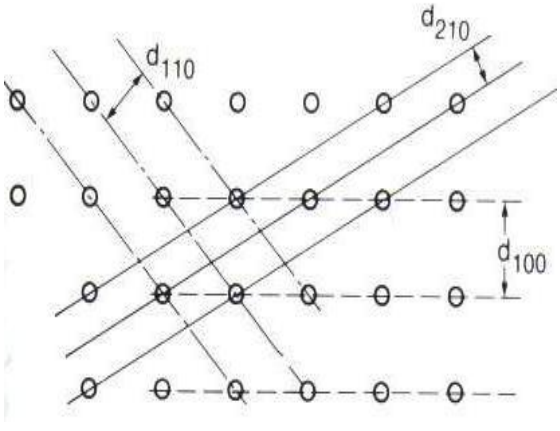

Figure 4.8 Spacing 'd'between planes.

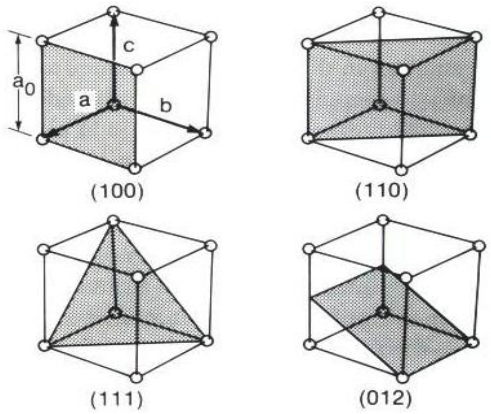

Figure 4.9 Planes in unit cell.

To distinguish between these, we introduce a coordinate system for the crystal whose unit vectors a, b, and c are the edges of the unit cell (Fig. 4.9). For the familiar cubic

crystal, these form an orthogonal system. Any atomic plane can now be uniquely distinguished by its Miller indices. These are the three reciprocal intercepts of the plane with a, b, and c axes and are reduced to the smallest integers having the same ratio. Thus, an (hkl) plane intercepts the crystallographic axes at a/h, b/k, and c/l; examples are shown in Fig. 4.9. The d-spacing between (hkl) planes is denoted d_{hkl}, and for cubic crystals, it is

$$\mathbf{d_{hkl}} = \frac{a_0}{\sqrt{h^2+k^2+l^2}}$$

where $\mathbf{a_0}$ is the lattice constant of the crystal.

When there is constructive interference from X-rays scattered by the atomic planes in a crystal, a diffraction peak is observed. The condition for constructive interference from planes with spacing d_{hkl} is given by Bragg's law:

$$\boldsymbol{\lambda = 2d_{hkl}\,Sin\theta_{hkl}}$$

where $\boldsymbol{\theta_{hkl}}$ is the angle between the atomic planes and the incident (and diffracted) X-rays beam (Fig. 4.7). For diffraction to be observed, the detector must be positioned so the diffraction angle is $2\theta_{hkl}$ and the crystal must be oriented so that the normal to the diffracting plane is coplanar with the incident and diffracted x rays so that the angle between the diffracting plane and the incident X-rays is equal to the Bragg angle θ_{hkl}. Knowing the angle of diffraction and wavelength of the incident X-Rays, d spacing between the planes can be determined.

4.4.1 Intensities of diffracted X -Rays

Before considering diffracted intensities, we first must consider X-Ray absorption, since this affects intensities. All materials absorb X-rays. Thus, an X-ray beam is attenuated as it traverses matter. The transmitted intensity decays exponentially with the distance traveled through the specimen and the linear absorption coefficient μ

describes this decrease. The absorption length (1/e decay length) is 1/ μ, and at λ = 1.54Å, typical values are 1mm, 66μm, and 4μm for carbon, silicon, and iron, respectively. Except near an absorption edge, μ increase with increasing atomic number and increasing wavelength.

Neglecting unimportant geometric factor,[1-3] the integrated X-ray intensity diffracted from a crystal is

$$\mathbf{I_{hkl} \propto |F_{hkl}|^{-2M} V}$$

Here $\mathbf{F_{hkl}}$ is the structure factor for the (hkl) diffraction peak and is related to the atomic arrangements in the material. Specifically, $\mathbf{F_{hkl}}$ is the Fourier transform of the positions of the atoms in one unit cell. Each atom is weighted by its form factor, which is equal to its atomic number Z for small 2θ, but which decrease as 2θ increases. Thus, XRD is more sensitive to high-Z materials, and for low –Z materials, neutron or electron diffraction may be more suitable. The factor e^{-2M} (called the Debye- Waller factor) accounts for the reduction in intensity due to the disorder in the crystal, and the diffracting volume V depends on μ.

4.5 Scanning Electron Microscope (SEM)

SEM provides the investigator with a highly magnified image of the surface of a material that is very similar to what one would expect if one could actually "see" the surface visually. This tends to simplify image interpretations considerably, but reliance on intuitive to SEM images can, on occasion, lead to erroneous results. The resolution of the SEM can approach a few nm and it can operate at magnifications that are easily adjusted from about 10× - 300,000×.

In SEM, a source of electrons is focused (in vacuum) into a fine probe that is rastered over the surface of the specimen, Fig. 4.10. As the electrons penetrate the surface, a

number of interactions occur that can result in the emission of electrons or photons from (or through) the surface.

A reasonable fraction of the electrons emitted can be collected by appropriate detectors, and the output can be used to modulate the brightness of a cathode ray tube (CRT) whose x- and y-inputs are driven in synchronism with the x-y voltages rastering the electron beam. In this way an image is produced on the CRT; every point

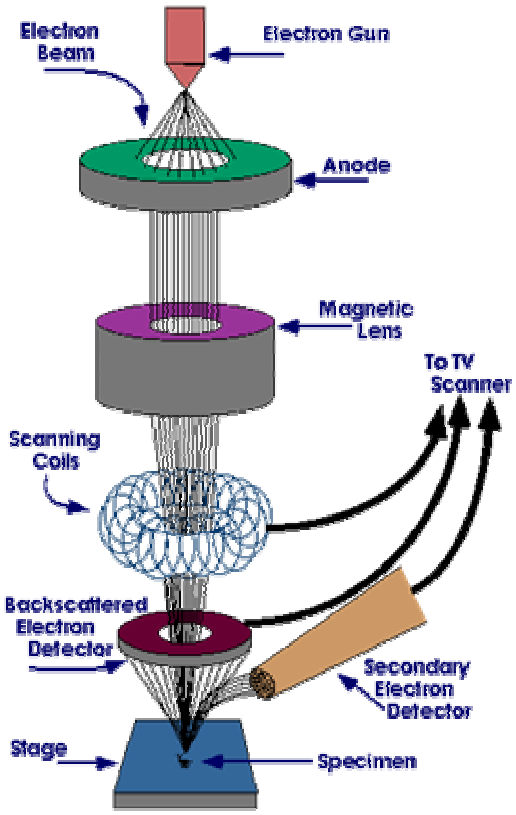

Figure 4.10. Schematic diagram for SEM working.

that the beam strikes on the sample is mapped directly onto a corresponding point on the screen. If the amplitude of the saw-tooth voltage applied to the x- and y-deflection amplifiers in the SEM is reduced by some factor while the CRT Saw-tooth voltage is kept fixed at the level necessary to produce a full screen display, the magnification, as viewed on the screen, will be increased by the same factor.

The principle images produced in the SEM are of three types: secondary electron images, backscattered electron images and elemental X-ray maps. Secondary and backscattered electrons are conventionally separated according to their energies. They are produced by different mechanisms. When a high-energy primary electron interacts with an atom, it undergoes either inelastic scattering with atomic electrons or elastic scattering with the atomic nucleus. In an inelastic collision with an electron, some amount of energy is transferred to other electron. If the energy transfer is very small, the emitted electron will probably not have enough energy to exit the surface. If the energy transferred exceeds the work function of the material, the emitted electron can exit the solid. When the energy of the emitted electron is less than about 50 eV, by convention it is referred to as a secondary electron (SE), or simply a secondary. Most of the emitted secondaries are produced within the first few nm of the surface. Secondaries produced much deeper in the material suffer additional inelastic collision, which lower their energy and trap them in the interior of the solid. Mostly secondary electrons are used in SEM for image formation.

An additional electron interaction of major importance in the SEM occurs when the primary electrons collides with and ejects a core electron from an atom in the solid. The excited atom will decay to its ground state by emitting either a characteristic X-Ray photon or an Auger electron as shown in Fig. 4.11 along with secondary electrons and back scattered electrons. A modern trend in electron microscopy is to fit X-ray analysis equipment as a bolt-on accessory. Bombarding a specimen with electrons causes X-rays of characteristic wavelengths and energies to be emitted from the spot where the beam strikes the specimen. Computer analysis of the wavelength (Wavelength Dispersive Spectroscopy) or energy spectra (Energy Dispersive

Spectroscopy) makes it possible to measure accurately the nature and quantity of different elements in the material.

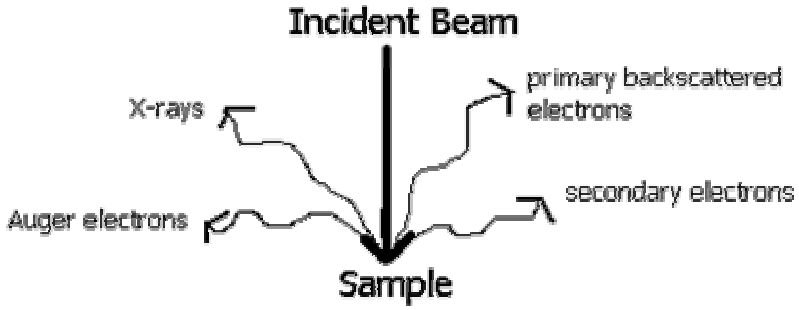

Figure 4.11 Reaction products when electrons are bombarded on specimen.

4.6 Planetary Mill

The "pulverisette laboratory planetary mill is universally applicable for quick dry or wet grinding of inorganic and organic samples for analysis, quality control, materials testing and mechanical alloying. In synthesis, it can be used for mixing and homogenization of dry samples, of emulsions and of pastes. The material is crushed and torn apart in two or four grinding bowls by grinding balls. The grinding balls and the material in the grinding bowl are acted upon by the centrifugal forces due to the rotation of the grinding bowl about its own axis and due to the rotating supporting disc. The grinding bowl and the supporting disc rotate in opposite directions, so that the centrifugal forces alternately act in the same and opposite directions. This results in, as a frictional effect, the grinding balls running along the inner wall of the bowl, and as an impact effect, the balls impacting against the opposite wall of the grinding bowl. The impact effect is enhanced by the grinding balls impacting against one another. Loss-free grinding, even in the case of grinding of suspensions, is guaranteed by a hermetic seal between the grinding bowl and the cover. Planetary mill along with rotating platform is shown in the Fig. 4.12.

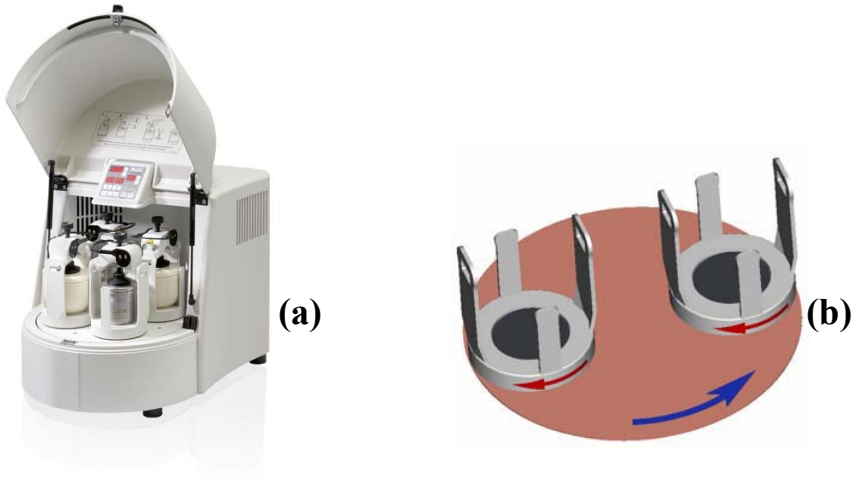

Figure 4.12. (a) Planetary Mill (b) Base of the planetary mill showing the rotation of platform and jars in opposite direction.

4.7 Laser Particle Size Analyzer

Laser particle size analysis is a versatile technique which is based on light scattering. Low angle Fraunhoffer light scattering using monochromatic (laser) light with dispersed particles is widely used for automatic size analysis. Particle size affects both the intensity and angular extent of scattering.[43] A fluid stream with dispersed particles is passed in front of a detector system. With coherent (laser) light the angle of scattering varies inversely with particle diameter as illustrated in the Fig. 4.13. The intensity of the scattered signal varies with the square of the particle diameter. Computer analysis of the intensity versus angle data will determine the particle size distribution. The smallest particles should be at least twice the wavelength of the laser light for detection. As with other approaches to particle size analysis, the particle shape is assumed to be spherical. Detecting agglomeration is difficult, but can be minimized by proper dispersion and ultrasonic deagglomeration. The schematic diagram for the instruments used in the present study is shown in the Fig. 4.14. The sample carrying liquid is circulated by the centrifugal circulation pump. The computer screen is used for displaying and setting the condition for measuring, retrieving, and displaying data. There are two light sources: a long-life 632.8 nm He-Ne laser

expanded by a beam expander and a tungsten lamp. The light from tungsten lamp is through the filter, and the light used is approximately 405 nm. The light emitted from the laser and the tungsten lamp is radiated on the particles suspended in the liquid. After the laser beam has been dispersed and scattered by the particles in the flow cell, it passes through the condenser lens and is focused on the forward ring silicon diode array, comprised of 75 separate detection elements. The scattered light from the tungsten lamp is sensed by 6 wide-angle silicon diode detectors, ranging in angles up to 138° from the forward direction. The intensity of this scattered light from both the laser and tungsten lamp is converted into electrical signals, which are then used to calculate the size distribution of the particles.

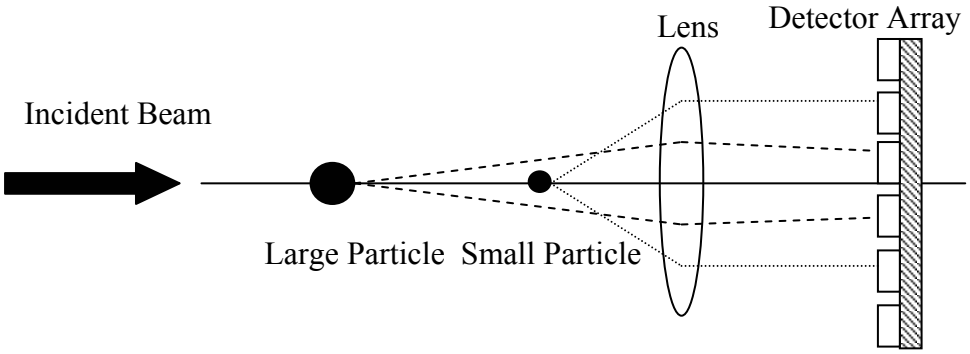

Figure 4.13. Small particle provide a wider scattering angle than large particles, giving a basis for particle size analysis.

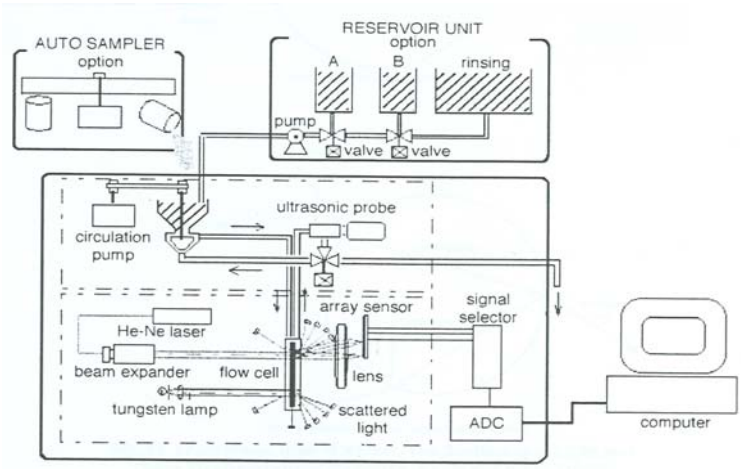

Figure 4.14. Schematic diagram for particle size analyzer (Model LA-920 Horiba, Japan) used in present study.

5 Experimental Procedures

PZT samples with 9 mole % Sr doping were prepared by mixing of oxides such as PbO, TiO_2, ZrO_2 and $SrCO_3$, according to the formulae $Pb_{0.91}Sr_{0.09}(Zr_{0.53},Ti_{0.47})O_3$ with 2.5 wt.% excess PbO to account for lead loss during calcination and densification. The process flow chart is shown in the Fig. 5.1. Purity and size of precursor powders with manufacturer information is given in table 5.1.

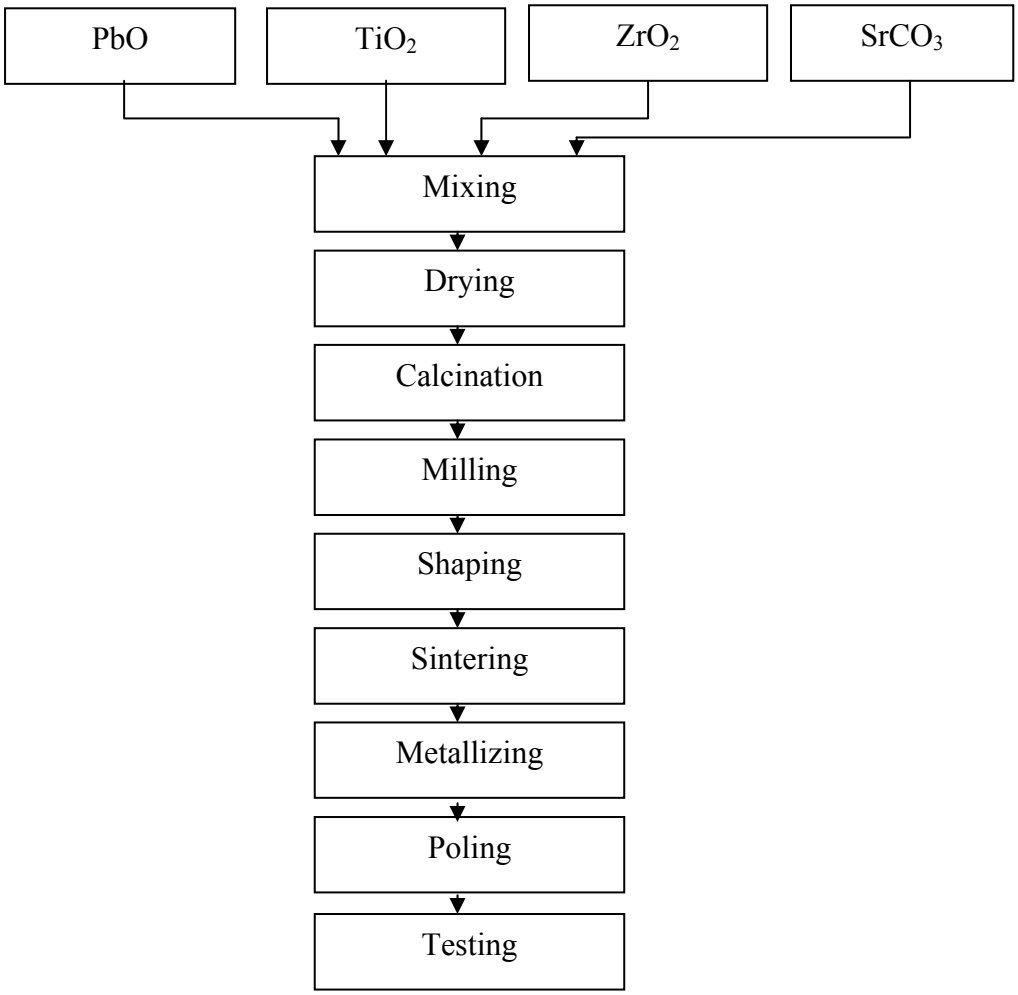

Figure 5.1. Flow chart for processing of PZT by mixed oxide route.

Table 5.1 Purity of precursor powders

Precursor	Purity (%)	Manufacturer
PbO	≥ 99.0	Fluka, Switzerland
TiO_2	>99.0	Riedel – de Haën ® Germany
ZrO_2	>99.0 (excluding 2% HfO_2)	Alpha Aesar
$SrCO_3$	>99.0	Alpha Aesar

5.1 Mixing and Drying

The powders in the appropriate mixing ratios were wet mixed with isopropanol in a planetary mill for 11 hours at 100 rpm. The rotation direction was reversed after 15 minute to get thorough mixing. Mixing was carried out in 250 ml WC bowls by using zirconia balls as grinding media. For 100 gram of powder forty five zirconia balls, diameter 15 mm, were used. Mixed powder was characterized by SEM analysis to check agglomerates and size distribution of powders. The powders were dried at 70 °C for 24 hours.

5.2 Calcination

Dried powder was pressed at 100 MPa in the shape of disc of size diameter 25 mm×10mm thickness and calcined at 850 °C for 2 to 15 hours in alumina crucibles

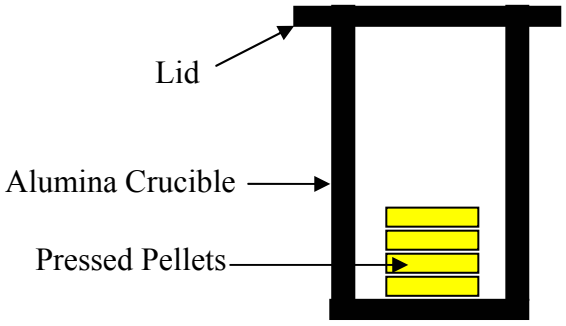

Figure 5.2. Scheme for calcination of pressed pellets.

covered with lid. Scheme of calcination is given in the Fig. 5.2. Heating rate was kept at 3°C/min followed by furnace cooling. Calcined powder was ground and then

characterized by XRD for perovskite phase and by SEM analysis for grain size and morphology.

5.3 Shaping

Calcined powder was mixed with 2% PVA binder in a planetary mill for 4 hours and then dried at 70°C. The powder was then passed through 150 μm sieve. Pellets of size, OD 13mm, ID 04 mm and thickness 5mm, were pressed at 180 MPa. Green compacts were analyzed by SEM to evaluate porosity distribution.

5.4 Debinding

During drying and calcining processes, frequently gases are produced within the ceramic part by water release, oxidation, decomposition of impurities, hydrates, or carbonates, and binder burnout. The rapid release of gases can cause the buildup of pressure within the green compact or nonuniform shrinkage: resulting in cracking, bloating, warping, or other defects.[44] To avoid these defects samples were heated to 600°C at a rate of 2 °C/min and hold for 4 hours to ensure complete removal of organic binder.

5.5 Densification

After debinding the samples were sintered at 1200°C for 2 hours in sealed alumina crucibles. Heating and cooling rate was maintained at 3°C/min. Pellets were surrounded by Pb rich powder to avoid PbO loss. Sealing was carried out by mixture of fine alumina powder and sodium silicate. The scheme of filling the crucible with surrounding powders is shown in the Fig. 5.3. A layer of plain PZT powder was laid around the pellet to be densified. After that plain PZT powder layer was surrounded by used PZT powder.

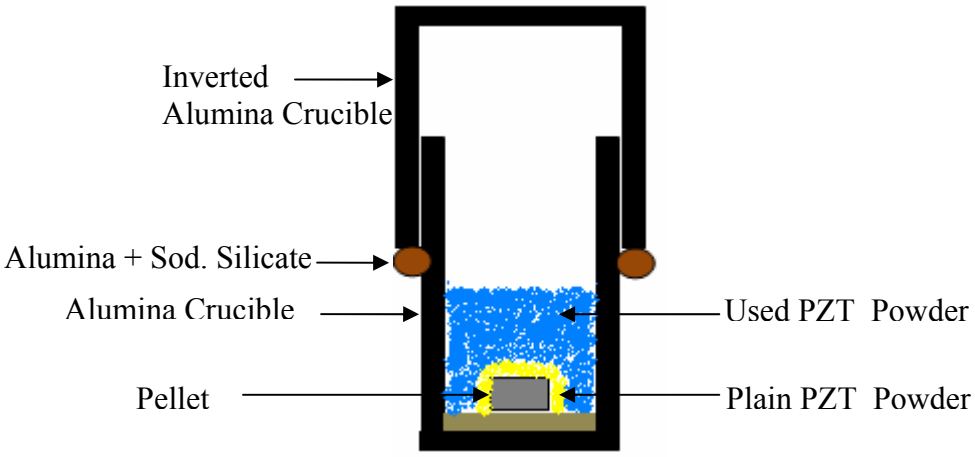

Figure 5.3 Scheme for densification of pellets.

5.6 Metallizing/Electroding

Sintered pellets were metallized using cermet silver conductor (ESL 599-E) purchased from Electro-Science Laboratories, Inc., USA. Cermet silver conductor in the form of paste was applied to samples using 325 mesh silk sieve. Pellets were dried with air heater at 100°C for 10 minutes and then fired at 550°C for 15 minutes with ascent/descent rate of 60°C/min. After firing the quality of coating was tested using multimeter.

5.7 Poling

Pellets were poled at 10 and 15 KV (2.3 and 3.5 KV/mm respectively) in silicon oil at 110°C for 20 minutes. Schematic diagram for poling is shown in the Fig. 5.4.

5.8 Electrical Properties Measurement and Characterization

Capacitance and dielectric loss was measured using Precision LCR meter at 1 KHz. Charge coefficient, d_{33} ,was measured by Piezometer at a frequency of 110 Hz. Static force (about 10N) was employed to clamp the test piece within the jaws while an

oscillating force of 0.25N used for measuring d_{33} coefficient. Coupling coefficient k and mechanical factor Qm was measured by using a Transducer Analyzer. Particle size and shape was characterized by SEM analysis (Jeol JSM 5910 LV Japan at 20 KV) and the crystal structures of calcined and sintered samples were determined using XRD equipment (Stoe Theta-Theta Diffractometer System STAD I Germany). Cu Kα was used as radiation source and Ni as filter. Particle size analysis was made by Laser Particle Size Analyzer, Model LA-920 Horiba, Japan. The instrument can measure in the range 20 nm-2 mm.

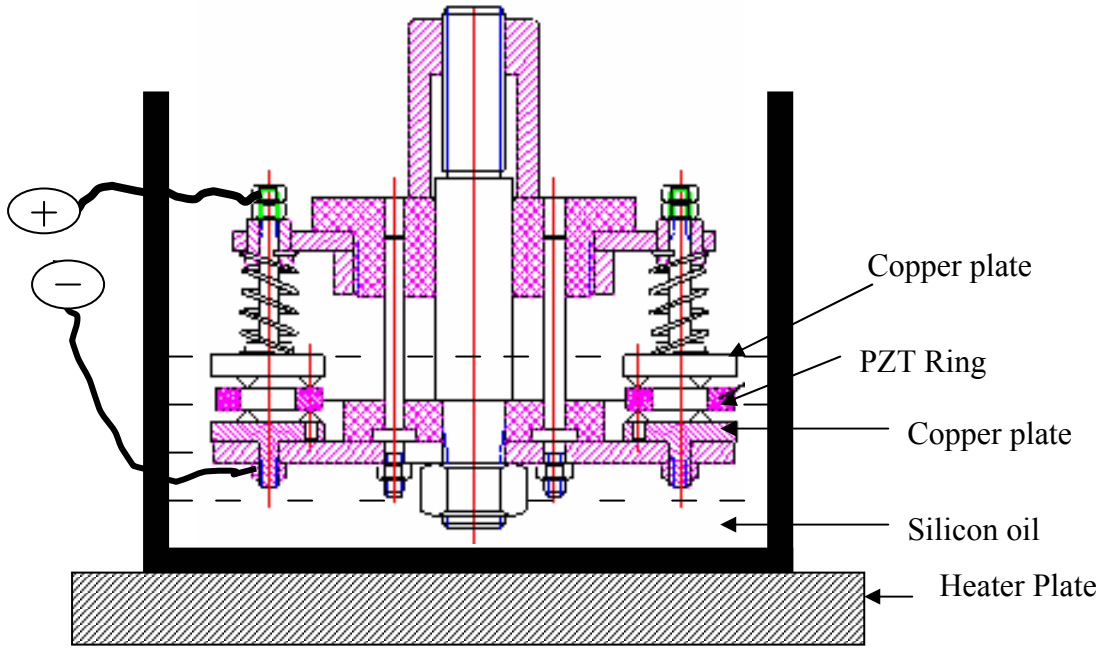

Figure. 5.4. Schematic diagram for poling of PZT sintered pellet.

6 Results and Discussion

6.1 Characterization of powders

At room temperature, the raw materials of PZT (PbO, TiO_2 and ZrO_2) exist in many polymorphic phases. Lead monoxide occurs in two polymorphic forms. One is litharge with tetragonal crystal structure, which is stable up to 450 to 550°C. In this structure, a layer of oxygen atoms lies between two layers of lead atoms, with the four oxygen atoms adjacent to each lead atom lying on the same plane. Therefore, each unit cell contains two PbO groups. The other, massicot, has an orthorhombic structure that has been described as a chain in which each lead atom is bonded to two oxygen atoms, and the chains are weakly bonded into layers by two lead-oxygen bonds of 2.49 Å length. There are four PbO groups per unit cell. It is stable above 500°C. The metastable massicot transforms readily to litharge by mechanical force although the additions of small impurities can stabilize the massicot form and prevent its transformation to litharge at ordinary temperature. Similar polymorphic forms exist in titanium dioxide such as stable rutile phase (a = 4.594 Å**,** c = 2.958 Å) and metastable anatase phase (a = 3.783 Å, c = 9.51 Å). The transformation of anatase to rutile occurs at about 1000°C. Both of these forms have tetragonal symmetry. The lattice of anatase is twice as large as that of rutile. Although there are three polymorphic phases of ZrO_2, the stable phase at room temperature is dependent on the amount of additives (e.g., MgO, Y_2O_3, or CaO). Therefore, the structure of ZrO_2 without any added stabilizer is always monoclinic phase. $SrCO_3$ has orthorhombic structure at room

temperature. There is also a rhombohedral form of $SrCO_3$ stable above 912°C. Precursor powders were characterized in terms of particle size and phase structure because these two properties greatly affect the calcination reactions. Finer the grain size, more active is the powder for calcination. Role of raw materials is discussed in the work by Sun-Yuan Chen *et al*.[45] Based on the work of Sun-Yuan Chen and others the sequence of reaction taking place in the formation of PZT and the effects of precursor powder characteristics (structure and reactivity) can be described as follows.

First reaction that occur during calcination is formation of $PbTiO_3$ from PbO and TiO_2[46]. PbO_{ss} is usually formed by solving $PbTiO_3$ into a PbO phase[47] and plays a role in the formation mechanism of $Pb(Zr,Ti)O_3$ solid solution. In the $PbO\text{-}ZrO_2\text{-}TiO_2$ system, the formation of PbO_{ss} phase is dependent on the kinds of ZrO_2 used. If the ZrO_2 constituent has a higher reactivity, PZT phase will be formed and PbO_{ss} phase formation is retarded or smeared out. The $PbTiO_3$ phase reacts with ZrO_2 instead of PbO_{ss} phase in this case, and the DTA peak corresponding to the formation of PbO_{ss} is depressed. When ZrO_2 with a lower reactivity is applied, the reaction of ZrO_2 with $PbTiO_3$ to form PZT needs more energy. If the formation temperature of PZT phase is higher than 800°C, PbO has a chance to react with $PbTiO_3$, and the DTA peak for PbO_{ss} formation is found at a higher temperature (about 745°C).[45] The influence of PbO_{ss} on the formation of PZT solid solution is shown in Fig. 6.1, where existing phases and their relative amounts are plotted against calcination temperature. Because ZrO_2 of higher activity (0.1 μm) is used, the PZT phase can nucleate at a relatively low temperature. When temperature is higher than 700°C, $PbTiO_3$ and PZT are the only observed phases, in the rutile TiO_2 case. In the case of anatase TiO_2, the presence of a certain residual massicot PbO phase makes the PbO_{ss} phase observable, but the

amount of PbO_{ss} and PZT phases at a given temperature is lower. It happens due to the fact that anatase TiO_2 makes the PbO_{ss} phase stable at relatively higher temperatures than rutile TiO_2. Therefore, the crystallization and piezoelectric properties of PZT ceramics are better when rutile TiO_2 is used.

It is also shown that amount of PbO_{ss} formed is higher when massicot PbO is present as compared to litharge PbO.

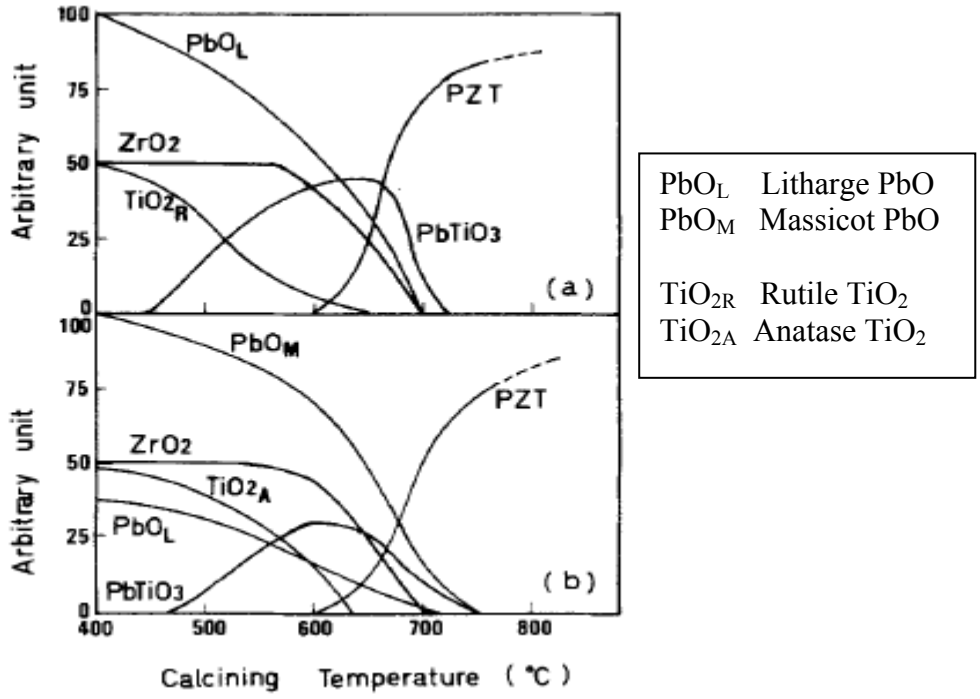

Figure 6.1. Reaction diagram of formation behavior of PZT versus calcining temperature for (a) rutile and (b) anatase TiO_2 added.

From the above discussion it can be concluded that finer ZrO_2, Rutile TiO_2 and Litharge PbO are better precursor materials for PZT fabrication.

In the present work the precursor powders were characterized in terms of particle shape, size, size distribution and structure by techniques such as SEM, laser particle size analyzer and XRD. SEM micrographs for all the precursor powders are shown in the Fig.6.2. In this figure it is shown that PbO has plate type particles and particle size range is 2-10. ZrO_2 powder is agglomerated with submicron particle size. TiO_2 is also

submicron but particle size is not revealed by SEM. $SrCO_3$ particles are also not clearly revealed by SEM.

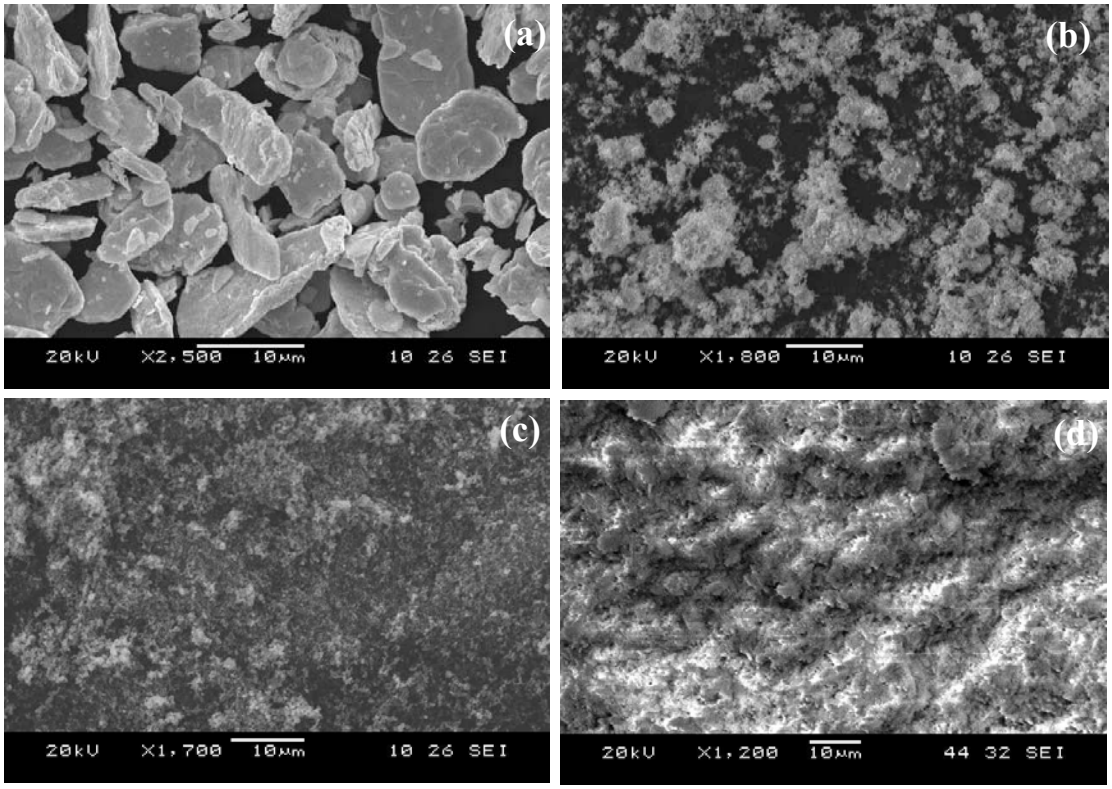

Figure 6.2 SEM micrographs of precursor powders. (a) PbO (b) ZrO_2 (c) TiO_2 (d) $SrCO_3$

Particle size analysis of the same precursor powders carried out by Horiba Laser Particle size analyzer to get precise particle size distribution and the results are shown in the Fig.6.3. In this figure it is shown that PbO has bimodal particle size distribution which is also seen in the SEM micrographs (Fig.6.2). In this distribution 30% of particles lie in the range of 0.3-1 µm and 70% lie in 1-10 µm range and mean size is 3.10 µm. ZrO_2 has mean particle size of 0.52 µm and TiO_2 is 0.18 µm. $SrCO_3$ powder has multimode particle size distribution (0.2-10 µm) with mean particle size of 1.6µm. The crystal structure of powders PbO, TiO_2, ZrO_2 and $SrCO_3$ was determined by XRD analysis. The XRD pattern for PbO is shown in the Fig. 6.4. All the peaks matches closely with ICDD (International Centre for Diffraction Data) card *01-077-*

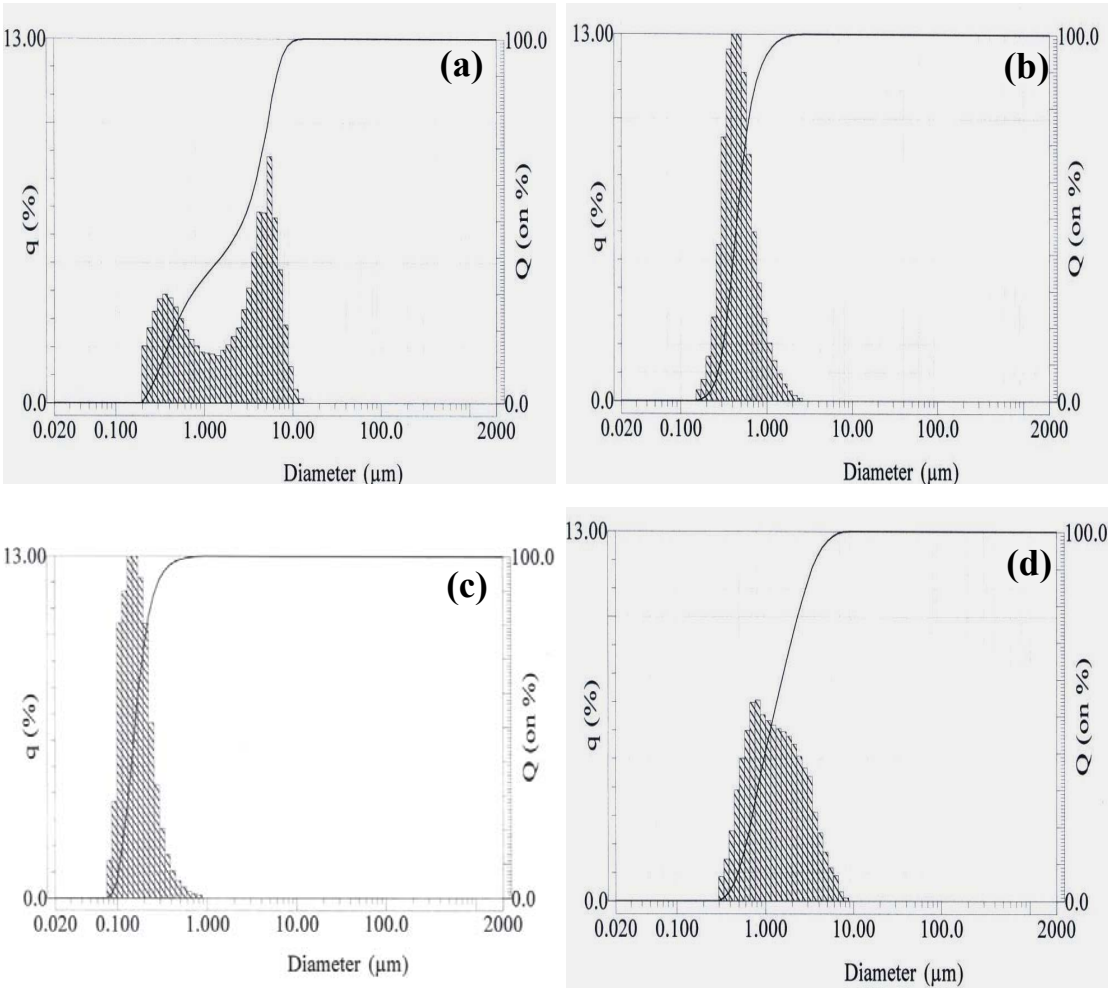

Figure 6.3. Laser particle size analysis of precursor powders (a) PbO (b) ZrO_2 (c) TiO_2 (d) $SrCO_3$.

1971 which gives that the structure of PbO is orthorhombic and precursor powder of PbO is designated as Massicot PbO . Similar XRD patterns for ZrO_2, TiO_2 and $SrCO_3$ are shown in the Fig. 6.5, Fig. 6.6 and Fig. 6.7 respectively. ZrO_2 is monoclinic matched with ICDD card *01-070-8739*, TiO_2 is tetragonal (anatase) matched with ICDD card *00-021-127* and $SrCO_3$ is rhombohedral matched with ICDD card *00-005-0418.*

Based on the visual inspection, SEM analysis and XRD of initial powders, features of the precursor powders are summarized in the table 6.1.

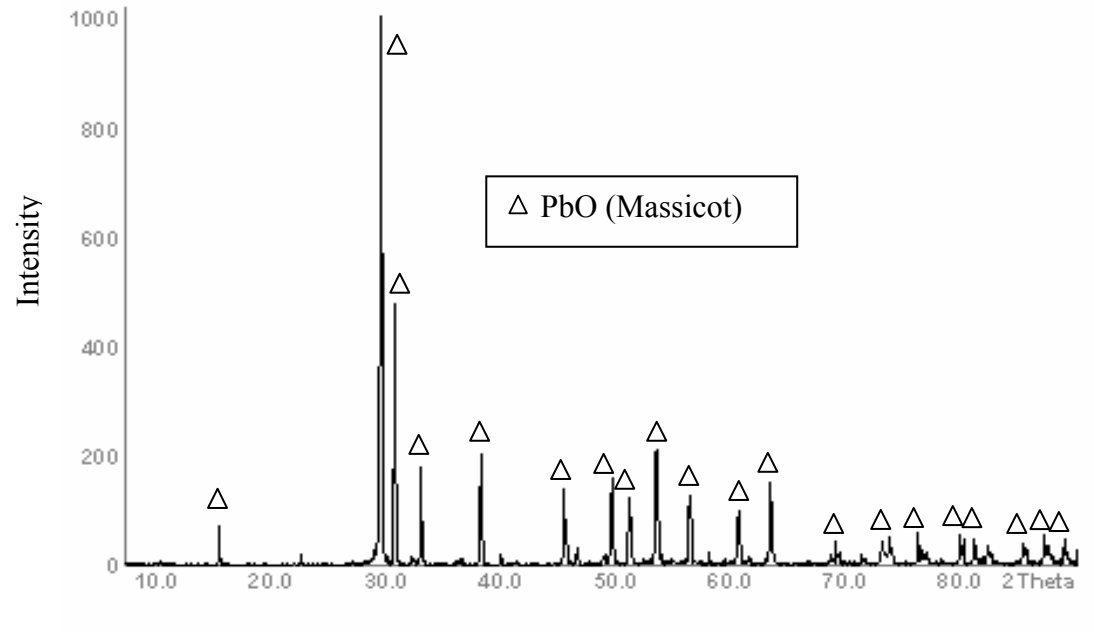

Figure 6.4. XRD pattern for PbO precursor powder.

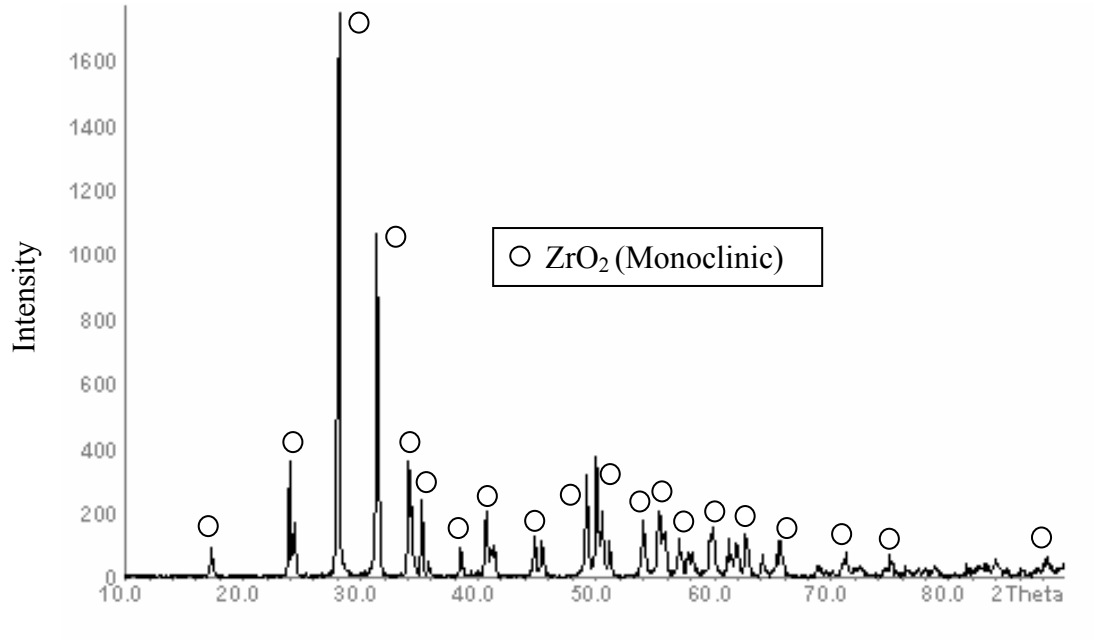

Figure 6.5. XRD pattern for ZrO_2 precursor powder.

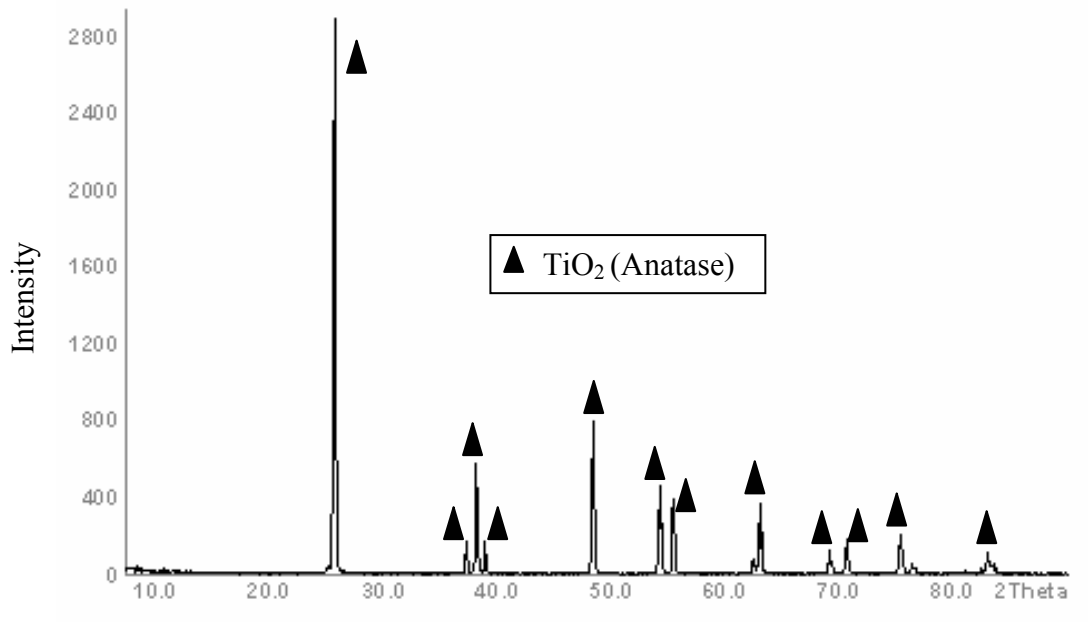

Figure 6.6. XRD pattern for TiO_2 precursor powder.

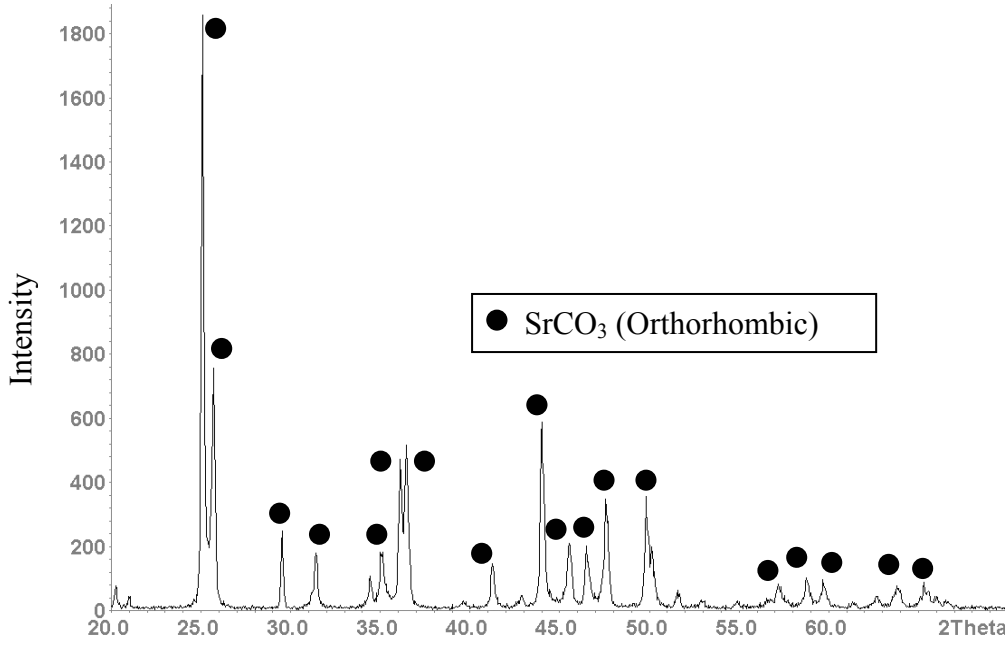

Figure 6.7. XRD pattern for $SrCO_3$ precursor powder.

Table 6.1 Characteristics of precursor powders based on XRD and Particle size Analysis.

Precursors	Color	Mean Size µm	Size Distribution	Structure
PbO	Yellow	3.10	Bimodal	Orthorhombic (Massicot, Syn.)
TiO_2	White	0.18	Gaussian	Tetragonal (Anatase, Syn.)
ZrO_2	White	0.53	Gaussian	Monoclinic
$SrCO_3$	White	1.66	Multimodal	Orthorhombic

6.2 Mixing

The precursor powders were wet mixed with isopropanol in a planetary mill for 11 hours. Mixed powders were dried and uniaxially pressed to pellets in the size of diameter 20 mm by 8 mm thickness for calcination. Cross sectional view of pellet after drying is shown in Fig. 6.8 (a). No large size porosity is seen in SEM micrograph (Fig. 6.8 a) which indicate that the particles are close to each other and calcination reaction will take place uniformly in all regions of the pressed pellet. Particle size and distribution of mixed powder is not clearly revealed, Fig. 6.8 (a).

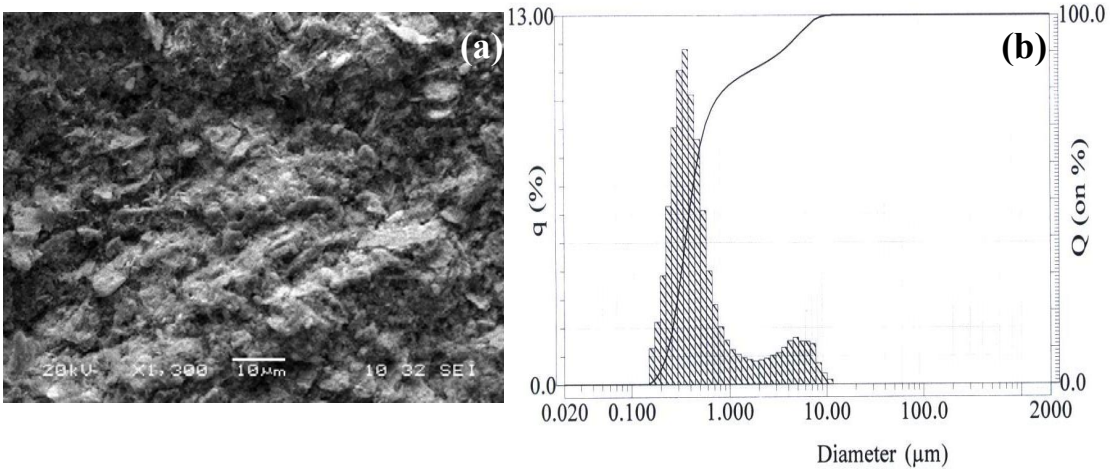

Figure 6.8 (a) Cross sectional view of pressed pellet prepared from mixed precursor powders. Mixing was carried out in a planetary mill for 11 hours. (b) Particle size distribution of mixed powders by laser particle size analyzer.

The same mixture of powders (after mixing) was subjected to laser particle size analysis and result is shown in Fig. 6.8 (b). In this figure it is seen that about 10% of particles are in the range 1 μm to 10 μm while about 90 % of particles are less than 1 μm. It is presumed that large particle sizes (1 μm to 10 μm) present initially in PbO precursor powder has not been reduced to fine size in the process of milling.

6.3 Calcination

Calcination of precursor powders after mixing in a mill was carried out for the formation of PZT phase (perovskite structure). In the literature a range of calcination temperatures for formation of PZT phase is reported. H. Zheng et al[10,11] has calcined at 925°C, C. Bodoya et al at 800°C. In present work, powders were calcined at 850°C and holding time was varied between 2 to 15 hours. Selection of calcination temperature at 850 °C was made due to the fact that formation of PZT phase complete at 830°C.[48] The extent of calcination of solid oxide powders has a direct influence on the later production of PZT ceramics. It is therefore necessary to check the phase and the microstructure of the calcined powder at this stage.

6.3.1 SEM Analysis

SEM profiles of calcined powders are shown in the Fig. 6.9(a-d). Calcination was carried out at 850°C for 2, 8 and 15 hours. Fig. 6.9(d) shows higher magnification of powder calcined for 15 hours showing formation of necks between the grains. Formation of necks at this stage may be attributed to presence of liquid PbO phase at the calcination temperature (850°C). An increasing trend in grain size is also observed when calcination time is increased from 2 to 15 hours Fig. 6.9(a-c). SEM micrographs in Fig. 6.9 (a-c) also show skeletal type structure after calcination. This structure is due to the fact that the formation of PZT (perovskite structure) is

accompanied by volume expansion because PZT phase has different molar volume than its component oxides.[49] The volume expansion in the formation of PZT from its component oxides necessitates that perovskite formation reaction should complete prior to sintering step since further morphological changes may hinder densification and overall homogeneity.

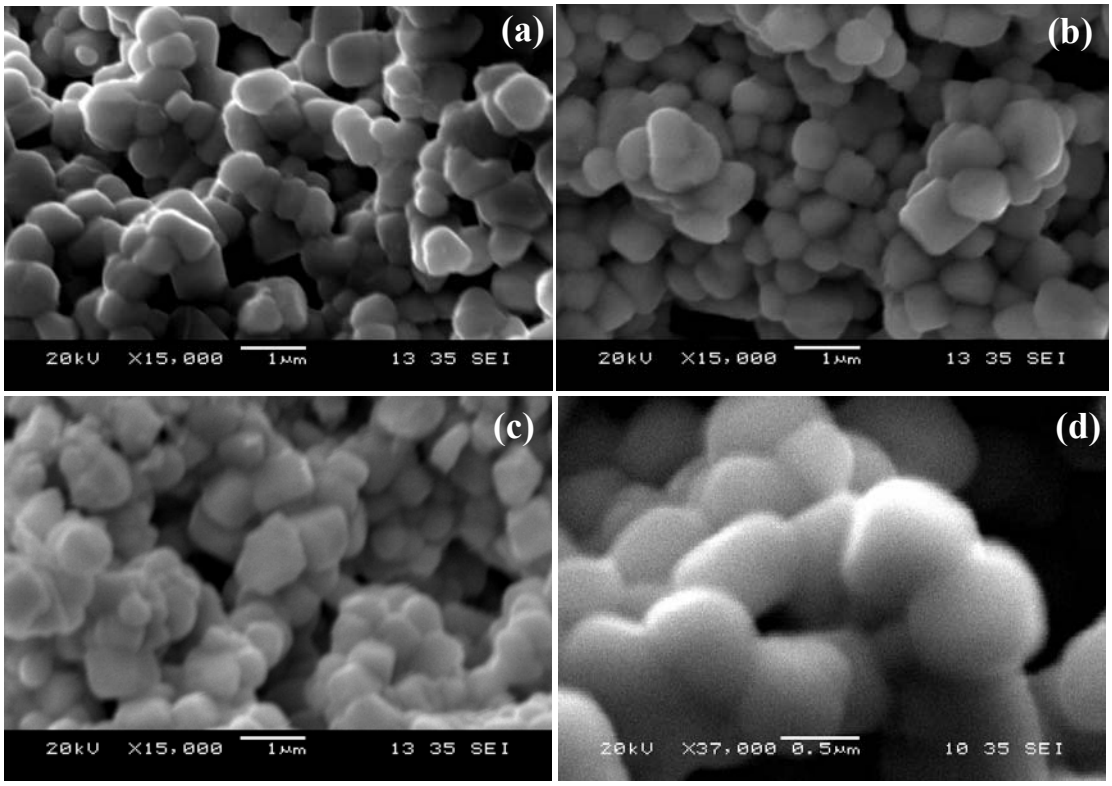

Figure 6.9 SEM micrographs after calcination of precursor powders: (a) 2 hours (b) 8 hours (c) 15 hours (d) Same as (c) but at higher magnification.

6.3.2 XRD Analysis

The calcined samples were subjected to XRD analysis to ensure complete formation of PZT phase (perovskite structure) and the detection of unwanted phases such as ZrO_2, PbO and PbO_{ss}. The XRD pattern for 2 hours calcination at 850°C is shown in the Fig. 6.10. The pattern was matched with ICDD card *01-070-4265*, $Pb(Zr_{0.53}Ti_{0.47})O_3$, which shows a rhombohedral symmetry. Except a small PbO peak at $2\theta = 29°$ all the peaks matches to this card which shows the structure is mainly

perovskite. Emergence of PbO peaks indicates that some unreacted or extra PbO added is present after 2 hours of calcination. Similar patterns for samples calcined at 8 and 15 hours are shown in the Fig. 6.11 and Fig. 6.12 respectively. After 8 hours calcination the intensity of PbO peak has reduced indicating that some PbO has evaporated or dissolved into PZT phase. When the sample was calcined for 15 hours PbO phase is not observed in XRD pattern as shown in the Fig. 6.12. After calcination at 850°C for 15 hours it is assumed that all of the excess PbO added has evaporated or dissolved in perovskite phase. One more trend that is observed is that intensities of the peaks increased gradually as holding time increased. The intensity of the reflection for plane (110) is 900, 1040 and 1200 for 2 hours, 8 hours and 15 hours calcination at 850°C. The increase in peak intensity is attributed to some initial sintering occurring at this temperature due to presence of liquid phase (PbO). Melting of PbO starts at 800°C. Presence of liquid phase at this temperature causes some necking between the grains and the grain boundary area starts decreasing. Because grain boundaries are considered as amorphous areas, the intensities of XRD reflections will increase slightly when the grain boundary areas decrease.

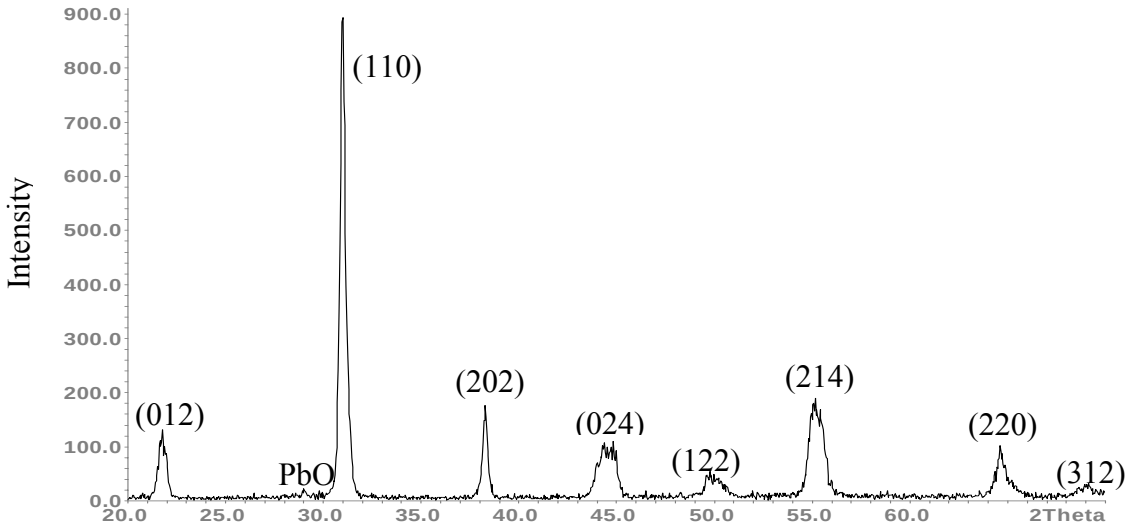

Figure 6.10. XRD pattern after 2 hours of calcination at 850°C.

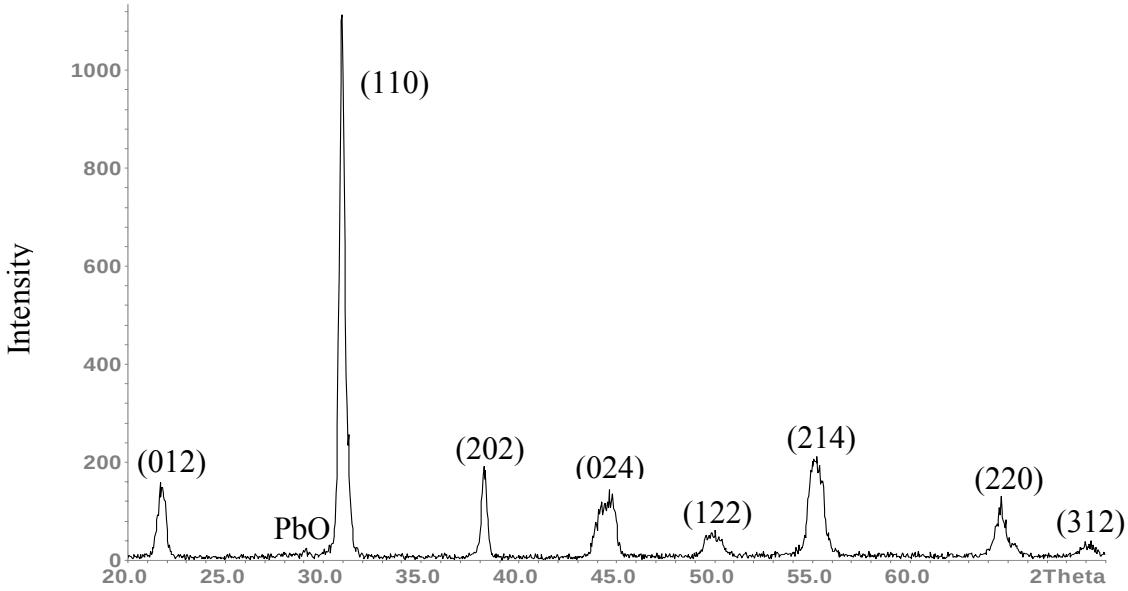

Figure 6.11. XRD pattern after 8 hours of calcination at 850°C.

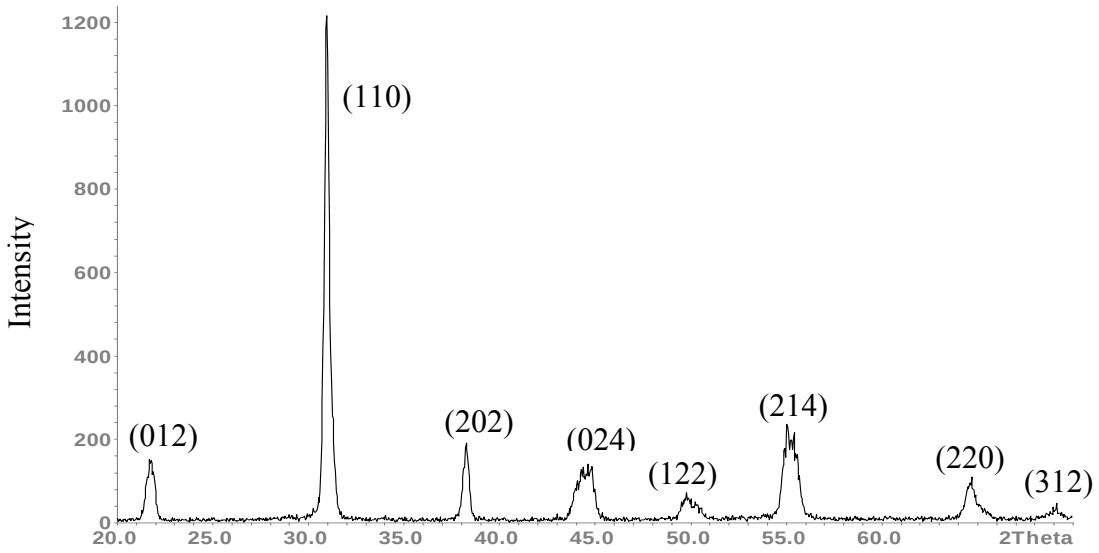

Figure. 6.12. XRD pattern after 15 hours of calcination at 850°C.

The increased contacts developed probably by grain growth are also manifested in the SEM profiles shown in the Fig. 6.9. All the XRD patterns show peak broadening. The same type of broadened peaks after calcination is observed in the work of Shue-Sheng *et al*.[31] Peak broadening decreases when the samples are sintered as shown in the Fig. 6.15. This peak broadening may be attributed to composition fluctuation in the solid solution and it will be discussed in detail in section 6.5.

6.4 Shaping

Calcined powder in the form of a pellet was first ground with mortar and pestle and then wet milled for 4 hours to break the contacts between the grains that were formed during calcination. Mixing of PVA binder with calcined powder was also done at this stage and then pressed to required shape. Shape and size of the powder particles after pressing are shown in the Fig. 6.13. Submicron to 1 μm size particles are observed in SEM micrograph taken at surface of the ring shaped sample as shown in Fig. 6.13 (a). Cross sectional view of the same sample is shown in the Fig. 6.13 (b). Some porosity is visible in the cross sectional view, Fig. 6.13 (b). Comparison of the powder sizes in the condition 'before calcination' (Fig. 6.8) and "after calcinations" (Fig. 6.9 and Fig. 6.13) exhibit that larger size particles, greater than 2 μm are not observed in the 'after calcination' condition. It means that the step of calcination in the PZT fabrication not only forms PZT phase but also reduce the particle size of the precursor powder.

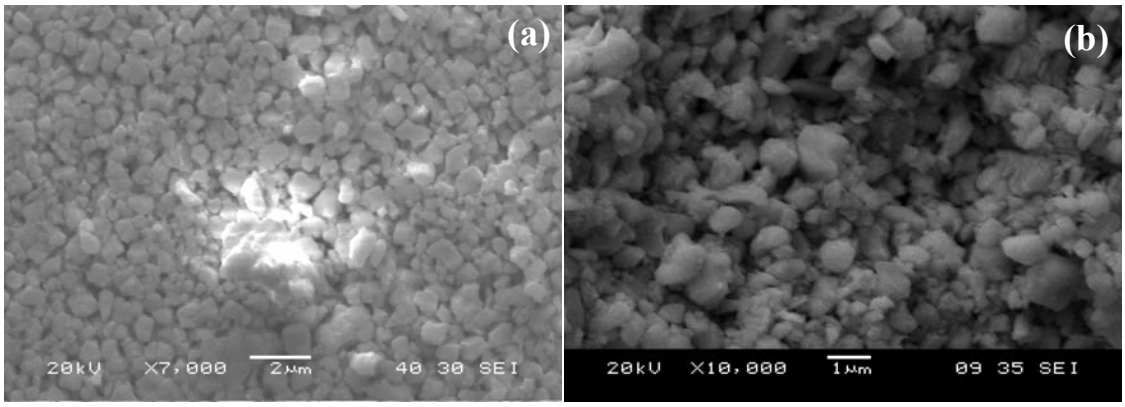

Figure 6.13. (a) SEM micrograph taken from the top surface of disc shape sample after compaction (b) Cross sectional view of the same sample taken after breaking the sample in the middle. Porosity is visible in cross-sectional view.

6.5 Densification

Densification or sintering is one of the most critical processing steps in the manufacturing of high density ceramic parts. This process becomes more complicated

by the presence of a volatile phase at the sintering temperature as in the case of PZT ceramics. PbO starts evaporating at 800°C. In order to decrease this evaporation, sintering is carried out in an atmosphere that has PbO activity equal to or greater than PbO activity in the sample material. However, some PbO loss is inevitable. The PbO loss is compensated by addition of 2-8 wt% extra PbO in precursor powders. Addition of extra PbO results in formation of liquid phase during sintering which helps in initial and intermediate stage of sintering by easy particle rearrangement and solution-precipitation but final sintered density decreases due to localized densification and formation of larger pores.[31,33] Deficiency of PbO, on the other hand, is accompanied by increase in defect concentration which enhances the densification in the final stage of solid state sintering.[33] It is also known that loss of PbO and resultant variation in composition affect the intrinsic electromechanical properties of the ceramic. In the present study sintering was carried out at 1200°C for 2 hours.

6.5.1 SEM Analysis

Fig. 6.14 shows SEM micrographs of samples after densification at 1200°C for 2 hours. Very dense structure is achieved at this temperature. Fig. 6.14(a) shows some porosity in the sample but the size of porosity is less than or equal to grain size (2-3 μm). The porosities less than grain size is normal feature in sintered parts in PZTs prepared by conventional slow heating cycle. However, low porosity may be obtained by fast firing.[15] But the technique of fast firing can not be applied to thick samples, therefore limiting its utility. Porosities considerably larger than the grain size are detrimental to mechanical strength as well as for dielectric and piezoelectric properties. Large porosities are source of initiation of cracks which develop during poling of PZTs.[50] In present work large porosities are not seen in the sintered microstructures (Fig. 6.14). Sintered and fractured samples reveal the morphology of

grain and mode of fracture, Fig. 6.14 (b-d). These SEM micrographs of the fractured surface of sintered samples are taken at different magnifications and locations. It is shown in the Fig. 6.14 (d) that the grain surfaces are very clean and no secondary phase is present at the grain boundary and the mode of fracture is mixed. Grain size is about 2-3 μm and no abnormal grain growth is seen. Size of the grains is uniform.

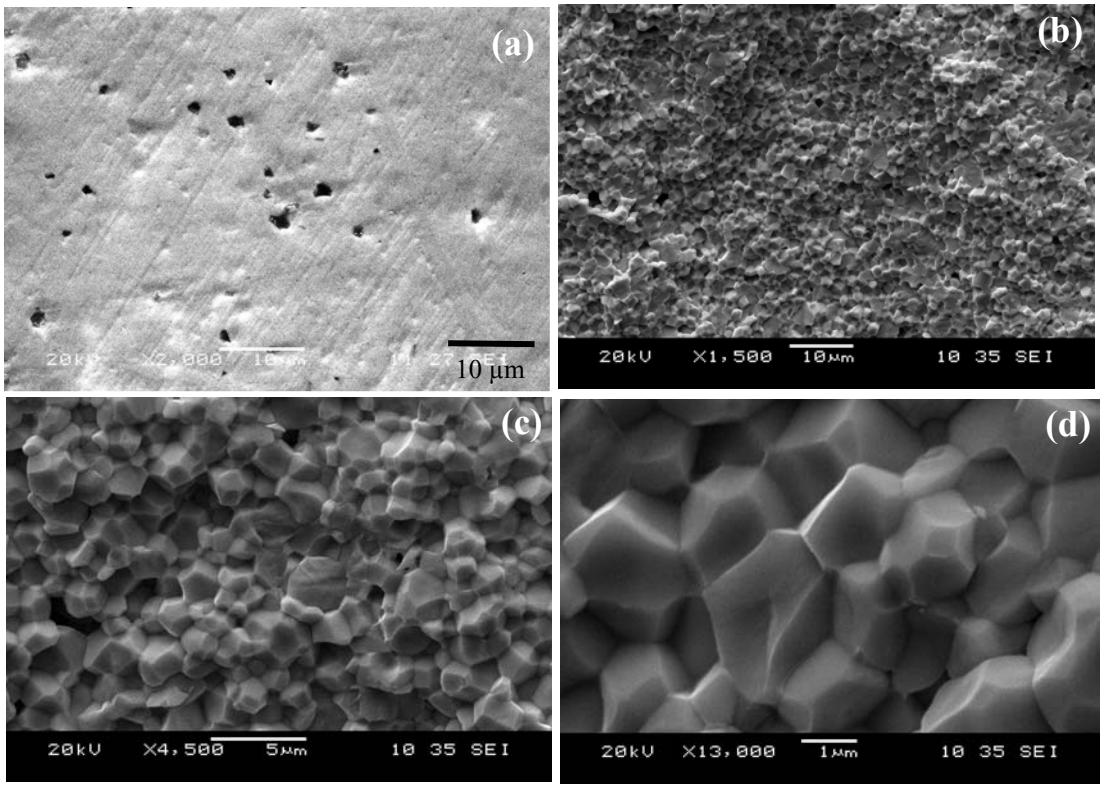

Figure 6.14 SEM micrographs after sintering (a) Polished surface 2000× (b) Fractured surface 1500× (c) Fractured surface 4500× (d) Fractured surface 13000×.

6.5.2 XRD Analysis

Sintered and poled pellet was ground to powder by mortar and pestle and was subjected to XRD analysis. XRD pattern is shown in Fig. 6.15. All the peaks correspond to PZT perovskite phase. Comparing of XRD patterns in calcined condition (Fig. 6.10 to Fig. 6.12) and sintered condition (Fig. 6.15), it is observed that broadened peaks of the planes (024), (122) and (214) in the calcined condition are replaced by two distinct peaks for each set of planes. Emergence of extra peaks in the

sintered condition (Fig.6.15) is due to better homogenization of structure at sintering temperature (1200°C). It may also be attributed to better removal of stresses and defects induced by milling of PZT powder in a planetary mill at the sintering temperature (1200°), while at calcination temperature (850°C) removal of these defects and stresses was not complete. Usually the sintering process enhances the electrical response of the ferroelectric ceramic via promotion of the ferroelectric phase and by increasing crystallanity. It is an over simplication to consider sintering as just densification. High temperatures associated with sintering complete the formation of the PZT phase and increase long-range order of the perovskite structure. With this in mind it must be considered that even if full densification could be achieved at low temperatures (by using sintering additives) and without resulting in an additional inactive second phase, it would still be expected that the final electrical properties of the sintered ceramic would be reduced as the atomic crystal structure would be less developed.

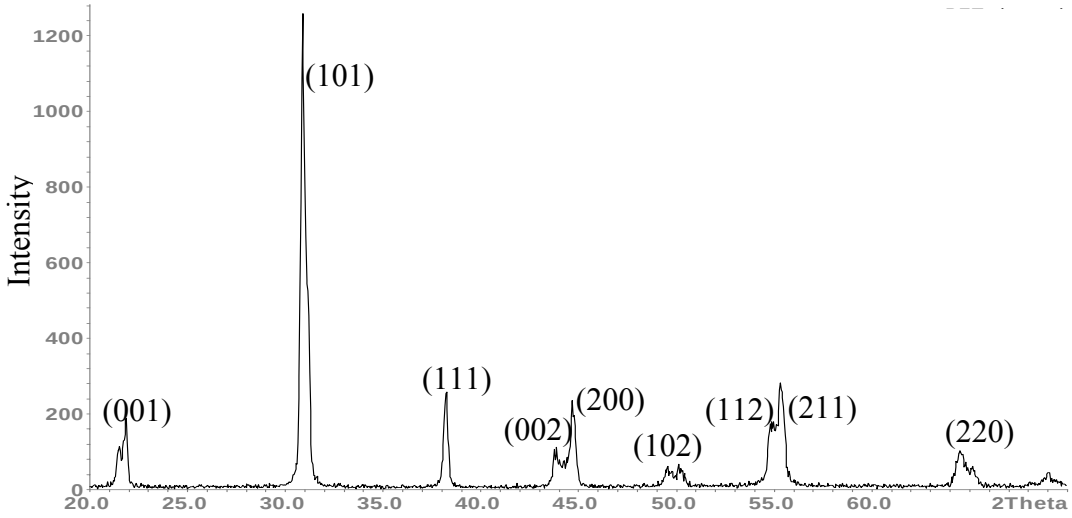

Fig. 6.15 XRD pattern for sintered, poled and ground PZT sample.

Reflections of plane (002) at 2 theta range, 43-46°, is of special interest. It is reported [51] that emergence of these reflections in the form of doublets and triplets takes place

in conventionally prepared ceramics due to compositional fluctuations leading to the coexistence of tetragonal and rhombohedral phases. If in this range two reflections $(002)_T$ and $(200)_T$ appear, the structure is considered to have tetragonal symmetry while appearance of third reflection, $(200)_R$, between the above two reflections indicates that PZT is consisted of both tetragonal and rhombohedral phases. By observation of Fig. 6.15 it can be concluded that the sintered structure is tetragonal. The researchers[9,30,51] has studied the 43-46° range as measure of compositional fluctuation and extent of domain switching by comparing relative intensities of these two reflections. The work of C. Budoya, Fig. 6.16, shows the change in relative intensities of the two reflections as the field is applied for poling. Before poling the reflection (200) has higher intensity as compared to (002) reflection. After poling at 2 KV/mm the condition is reversed such that (002) reflection has now higher intensity due to switching of 90° domain walls. In his work when the sample was annealed at 800°C, the relative intensities again exhibited the first trend. In the present work XRD analysis was taken after grinding the sintered and poled pellet with the help of mortar and pestle. Relative intensities of the two reflections in present work correspond to the condition of unpoled and poled+annealed condition in C. Budoya work. Here it is presumed that the grinding of sintered and poled pellet has the same effect as if it was annealed. It can be further explained in a way that when the poled sintered body was ground, the stresses induced by 90° domain switching in poling were relieved. It happened due to the fact that in the form of free particles, in contrast to polycrystalline body, the clamping force exerted by adjacent grains was no more applicable and the ground powder behaved as if it was annealed or not poled. To confirm this assumption, the sintered and poled pellet (without grinding) was also analyzed by XRD (Fig.6.17). Before XRD analysis the pellet was dipped in HCl for a

few seconds to strip off the silver electrode. Fig. 6.17 exhibits the XRD reflections in which the intensity of reflection $(002)_T$ has increased and the intensity of reflection $(200)_T$ has decreased indicating that 90° domain switching occurred during poling and it reverted to normal tetragonal symmetry (Fig. 6.15) when it was ground. From here it can be concluded that grinding the sintered pellet has the same effect as of annealing.

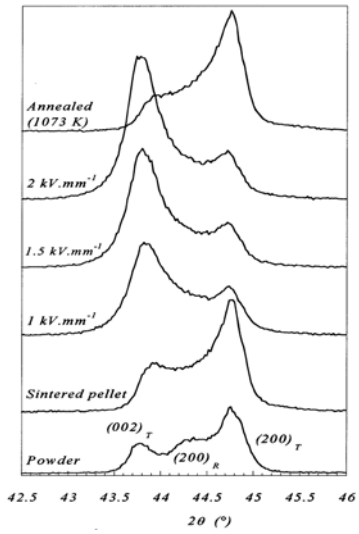

Fig. 6.16. Relative intensities of reflections as function of poling field.[9]

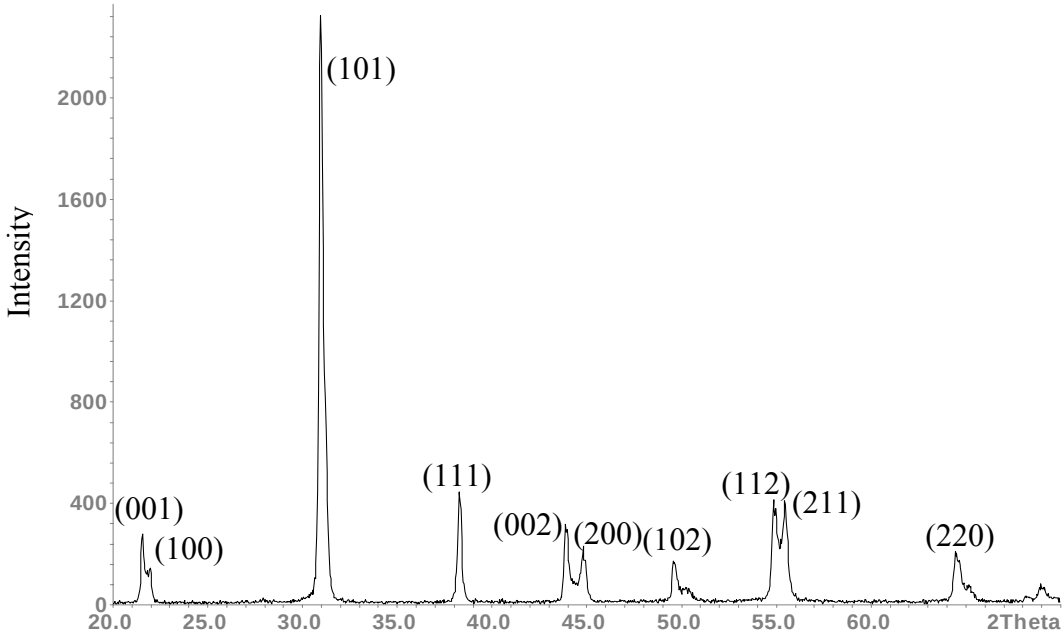

Fig. 6.17 XRD pattern for sintered and poled PZT sample.

For a tetragonal crystal system, the lattice constants a_T and b_T have the same value, which is different compared to the lattice constant c_T. Therefore, the multiplicity of the $F_{(200)}$ peak intensity will be twice that of the $F_{(002)}$ peak intensity such that $I_{(002)} / I_{(200)} = 0.5$. In the present work intensity ratio calculated by height of these two reflections in the condition when the pellet was ground to powder is as follows.

$I_{(002)} / I_{(200)} = 102.4/203.2 = 0.504$ (Neglecting the complex intensity factors).

It is also reported[52] that the switching of 90° domain in PZT ceramics can also be produced at the surface of sintered sample by mechanical forces such as grinding and polishing.

Calculation of lattice parameter (sintered+poled+ground) was done with (002) and (200) reflections using Si (99.99%) as internal standard and the results are given in table 6.2. For comparison the lattice parameters for the ICDD card *01-072-7169* used for matching of the sintered structure is also given. The composition of PZT for this card is $Pb(Zr_{0.525}Ti_{0.475})O_3$. Tetragonality (c/a ratio) calculated is 1.018. Same tetragonality is expected in sintered+poled condition due to the fact that domain switching does not change tetragonality.

Table 6.2. Lattice parameters of ground powder of sintered and poled pellet in comparison with ICDD card used for matching sintered and poled structure.

Sample/Card	Lattice Parameter (Å)		Ratio c/a	Symmetry	Unit Cell Volume Å^3
	c	***a***			
Ground Powder of Sintered and Poled Pellet	4.1254	4.0524	1.0180	Tetragonal	67.747
ICDD card used for matching sintered structure	4.1230	4.0440	1.0194	Tetragonal	67.400

6.6 Composition Analysis

Composition of sintered sample was measured on SEM equipped with EDX. Composition of sintered sample along with theoretical (stoichometric) composition for $Pb_{0.91}Sr_{0.09}(Zr_{0.53}Ti_{0.47})O_3$ is given in the table 6.3 without reporting oxygen content. The reason for omitting the oxygen content is due to the fact that oxygen being low atomic weight atom, EDX analysis of the solid solution will not be accurate. EDX used in present study is meant for analysis of elements with atomic number greater than 11.

Table 6.3. Composition of sintered part determined by EDX analysis and that of theoretical formulae $Pb_{0.91}Sr_{0.09}(Zr_{0.53}Ti_{0.47})$ used for preparation of starting composition.

Element	Composition of Sintered Part, %Atomic.	Theoretical Composition for $Pb_{0.91}Sr_{0.09}(Zr_{0.53}Ti_{0.47})$, % Atomic
Pb	43.13 ± 0.13	45.5
Zr	24.99 ± 0.35	26.5
Ti	27.40 ± 0.50	23.5
Sr	4.47 ±0.40	4.5

In undoped PZTs Zr/Ti ratio has limits for tetragonal and rhombohedral structures. If Zr/Ti ratio is > 1.127 the structure is rhombohedral and for Zr/Ti ratio < 1.127 the structure is tetragonal. At the ratio Zr/Ti = 1.127, structure is both tetragonal and rhombohedral. In this work Zr/Ti ratio calculated from EDX analysis (table 6.3) is 0.905 which shows it is tetragonal structure. Same tetragonal structure is evident from XRD analysis. Composition of sintered part (table 6.3) is deficient in lead as compared to stoichiometric (theoretical) composition which indicates that some lead oxide has evaporated during sintering. The observation of sintered microstructure in Fig. 6.14 shows that it is a very dense structure with a few porosities. It is reported that deficiency of PbO (less than stoichiometric amount) increases the final stage

sintering process. Higher the defect concentration, created by lead oxide deficiency, higher is the final density. In the present study it is assumed that final stage of sintering is oxygen vacancy-diffusion limited resulting in a highly dense structure. ZrO_2 content determined by EDX analysis (table 6.3) shows 1.6% deficiency than the stoichiometric amount. This deficiency may be attributed to presence of 2 % HfO_2 in the ZrO_2 precursor powder (table 5.1). It is known that chemically Zr^{+4} and Hf^{+4} have similar chemical characters. They have same charge (+4) and ionic radii are 0.072 nm for Zr^{+4} and 0.071 nm for Hf^{+4}. Binary system $Pb(Ti,Hf)O_3$ has a morphotropic phase boundary entirely analogous to that of $Pb(Ti,Zr)O_3$ and variation of dielectric constant (K) and coupling coefficient (kp) in both systems is same. Therefore it is expected that 2% HfO_2 in ZrO_2 precursor powder will not affect dielectric and piezoelectric properties in the final product.

6.7 Poling and Resultant Ferroelectric Properties.

Poling is very important step in the manufacturing of PZT ceramics in which domains are aligned in the direction of poling field. Variables that affect the poling process are field, temperature and time. Any increase in these variables will enhance the poling but increase is limited by dielectric strength of the material and development of microcracks due to generation of stresses during poling that will ultimately result in failure of the specimen. Therefore the poling process has to be optimized for each composition. Sintered pellets were poled at 2.3 and 3.5 KV/mm in silicon oil at 110°C. Dielectric and piezoelectric properties measured at above mentioned field strengths are shown in the Fig. 6.18. Before poling condition is represented as property at zero field. It is shown in the figure that the field of 2.3 KV/mm is sufficient to get optimized dielectric and piezoelectric properties such as dielectric constant, tangent loss, coupling coefficient and charge coefficient d_{33}. Comparison of

properties between present work and C-C-Hsueh et al is given in the table 6.4. C-C-Hsueh et al[16] has worked on the same composition as used in present work but with different heating cycle. The values are taken 24 hours after poling in both studies. In present work higher dielectric constant is achieved than the work of C-C-Hsueh. High dielectric constant in the present work may be due to better mixing by the use of a planetary mill for long times (11 hours). Two way action (the jar rotate in one direction and the platform in the other) in this mill gives better mixing in shorter times. Mixing process was further improved by reversing the direction of rotation after 15 minutes during milling time. Dielectric and piezoelectric properties generally suffer if there is any lack of homogeneity.

Table 6.4. Comparison of properties achieved in the present work and C-C-Hsueh *et al* work.

	Density g/cm^3	**Dielectric Constant (k)**	**Tangent Loss (Tanδ)**	**d_{33} (pC/N)**	**Coupling Coefficient**
Present Work	7.55	1440	0.0062	335	0.37
C-C-Hsueh *et al* Work	7.48	1300	0.025	325	0.53 (kp)

Lower dielectric loss (Tan δ) achieved in the present work as compare to work of C-C-Hsueh may be attributed to small grain size[14] obtained in the present work. For 6% Sr doping in PZT the reported value[14, 2] for dielectric loss (Tan δ) is 0.004 and for 9% Sr doped PZT the value of dielectric loss (Tan δ) is only reported by C-C-Hsueh. In the present work (9% Sr doped PZT) Tan δ = 0.0062 is slightly higher than 0.004 which is the reported[2,14] value for 6% Sr doped PZT. The increase in dielectric loss (Tan δ) in the present work (9% Sr doped PZT) is in accordance with the fact that Sr doping increases both dielectric constant and dielectric loss in PZTs. The work of C-C-Hsueh shows anomalously very high value for dielectric loss (Tan δ) = 0.025 which is an order of magnitude larger than the present work (0.0062) and reported value

(0.004)[2,14] for 6% Sr doped PZT. Charge coefficient (d_{33}) has almost same value in both works. Coupling coefficient (k) is lower (0.37) in the present work than the work of C-C-Hsueh. Dielectric constant (K), Tangent loss (Tan δ) and charge coefficient (d_{33}) are dimension independent parameters while the coupling coefficient (k) and mechanical quality factor (Q_M) are dependent on dimensions and shape of the specimen. Dimensions of the samples used for measurement of dielectric and piezoelectric properties are quite different in both works. In the present work a ring shaped specimen (OD = 11.60 mm, ID = 4.05 mm, Thickness = 4.32 mm) and in C-C-Hsueh work a disc shape specimen (diameter 10 mm and thickness 0.75 mm) were used. Therefore, the values of coupling coefficient are different in both cases. To further clarify this point let us check how it is measured. Measurement of coupling coefficient (k) is carried out by finding antiresonant and resonant frequencies using the following formulae

$$\mathbf{k} = \sqrt{\frac{F_a^2 - F_r^2}{F_a^2}}$$

where F_a and F_r are antiresonant and resonant frequency of the specimen. In general terms F_a and F_r depends upon the geometry and composition of the specimen. It means that for two samples, having the same composition, kp will be different for different geometry. In this work better dielectric and piezoelectric properties are achieved through conventional sintering practice. Reason for better properties (K, d_{33}, tangent loss) may be attributed to slightly higher density and better homogeneity in the present work. The density and grain size dependence of dielectric and piezoelectric properties has been explained by a space charge model for ferroelectric ceramics.[53] Relaxation of electrical polarization takes place due to development of polarization field at space charge sites such as lattice vacancies or impurity atoms

which are bound inside grain boundaries or domain walls. The smaller the grain size or higher the porosity, the larger the amount of grain boundary phase within a poly crystalline ceramic, so a stronger depolarization field will be created. The grain size

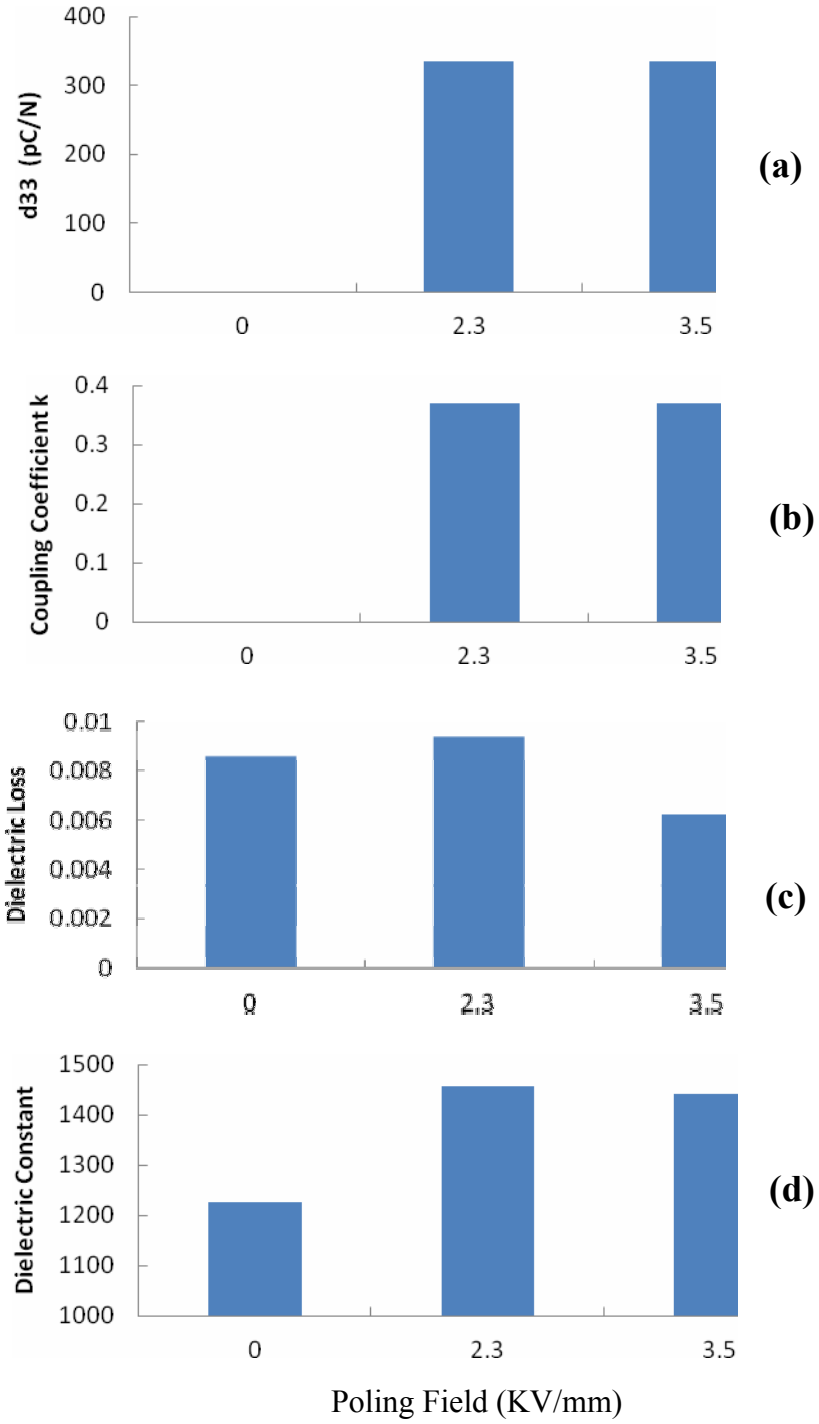

Figure 6.18. Piezoelectric and dielectric properties as a function of poling field (a) charge coefficient d_{33} (b) coupling coefficient (c) dielectric loss (d) dielectric constant.

effects has also been studied extensively by Clive A Randall et al in the size range of 0.1-10 μm. They[14] have reported that by increasing grain size, K, kp, d_{33} and Tanδ increase. In this work the grain size is about 2-3 μm, therefore, there is room for improvement in dielectric and piezoelectric properties by increasing grain size through manipulation on sintering time and temperature. However, it should be kept in mind that increasing the grain size will decrease the fracture toughness.[54] Present work (PZT doped with 9% Sr) has exhibited larger values for K and d_{33} than the reported[2,14] values for PZT doped with 6% Sr. Increase in K and d_{33} values was expected due to the fact that substitution of Sr. in PZT lowers the curie point and contribute to higher room temperature values for K and d_{33}.

6.8 Ageing Behavior

Although processed to yield excellent piezoelectric properties, PZT suffers from a long term ageing process in which piezoelectric properties decrease 0-5% per decade[13.] This means that if polarization of PZT decreases 5% by the first day, it is expected to have decrease 10 % by the 10^{th} day and 15% by the 100^{th} day and so on. Ageing is defined as spontaneous decrease of a property with time under zero external electric field and isothermal condition. This ageing is due to a diminution of domain wall mobility through the gradual build up of inhibiting causes. These may be internal fields due to alignment of dipoles formed from lattice defects and impurity ions, redistribution of internal strains due to crystal anisotropy or the accumulation of defects in the domain walls. It is reported for the $BaTiO_3$ system that during ageing dielectric constant, dielectric loss and coupling factors decrease while mechanical Q, elastic stiffness and frequency constants increase. For PZT systems, the same decreasing trends with time in the properties like dielectric constant, planar coupling factor (kp) and piezoelectric coefficient (d_{33}) are reported. The ageing effects can be

increased and properties stabilized by heating the specimens at 80°C for $BaTiO_3$ system and even higher for PZTs because PZTs have higher Curie temperature. In the present work, ageing behavior of poled samples for the time range of 1-84 days is shown in the Fig. 6.19. For the first 11 days the samples were aged at room temperature (25˚C). The samples were then kept in an oven for five days (12-16 days after poling in Fig. 6.19) at 50°C and then at 100 °C for three days (18-20 days after poling) to study accelerated ageing effects. Same decreasing trends in the properties K, kp and d_{33} were observed as reported by researchers for PZT system. In addition to general drop of these properties with time, a sharp decrease in d_{33} and k and an increase in K and Tangent Loss occurred when specimens heated at 50°C and 100°C. Increase in the value of K and Tangent Loss after heating at 50°C and 100°C is in accordance with the fact that all PZTs show maximum of these properties when approach Curie temperature (about 350°C).[2,17] On the other hand kp and d_{33} continue decreasing trend. Heating the specimen has a depolarizing effect caused by relaxation of stresses at elevated temperature. Therefore a sharp decrease in Kp and d_{33} is observed. Results for total change in properties after 84 days of ageing, for first 28 days of ageing and last 56 days of ageing are given in the table 6.4. Last 56 days are recorded separately to evaluate the change in properties when the sample was heated at 100°C. It is evident in Fig. 6.19 and data given in table 6.4 that all the properties are being stabilized when the sample was heated at 100°C (28 days after poling) which is in accordance with the reported fact. Charge coefficient (d_{33}) has decreased to a larger extent than dielectric constant (K) and coupling coefficient (k). The work of Sutham Sriloask has also reported higher degree of ageing in d_{33} as compared to K and kp in Sr doped PZT but the difference between his[13] work and the present work is

the extent of doping. In the present work PZT is doped with 9 % Sr as compared to 6% Sr in Sutham Sriloask's[13] work.

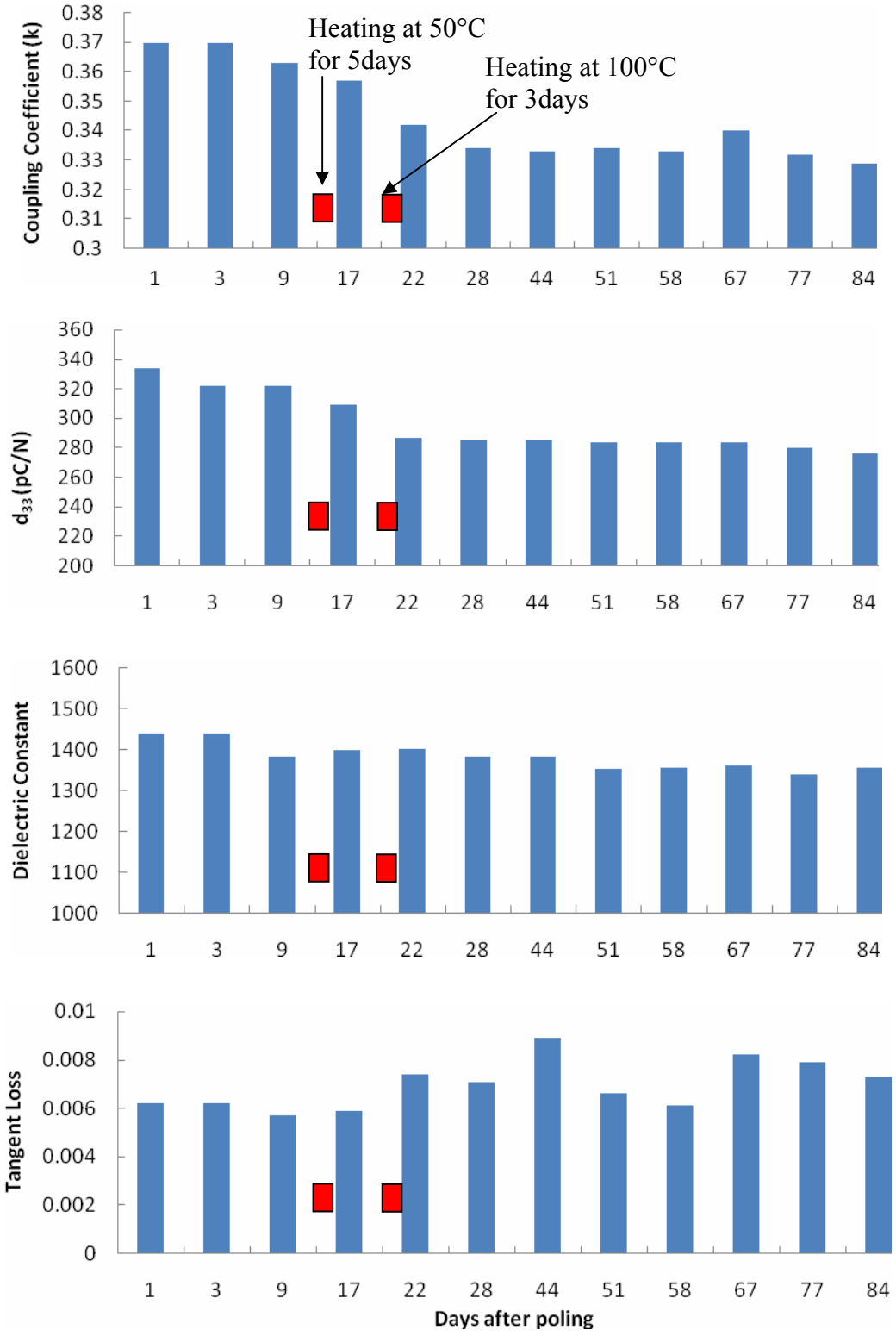

Figure. 6.19. Ageing behavior of dielectric and piezoelectric properties up to 84 days after poling.

Table 6.4. Change in properties for first 28 days, for last 56 days and total change in 84 days after poling.

Property	Change in Properties for first 28 days	Change in properties after heating at 100°C for 03 days (Data for last 56 Days)	Total Change in Property (Data for 84 days)
Coupling Coefficient (k)	9.5 % decrease	1.5 % decrease	11% decrease
Charge Coefficient (d_{33})	13.5% decrease	3.5 % decrease	17 % decrease
Dielectric Constant (K)	4.5% decrease	1% decrease	5.5 % decrease
Dielectric Loss	12% increase	2.5 % increase	14.5% increase

It is reported [55,56] that acceptor doping, e.g., Mn, and isovalent doping, e.g., Sr doping, slightly decreases aging rates of PZT, whereas donor doping, e.g., Nb, significantly decreases the aging rate of PZT. Doping of PZT with Sr also reduces the curie point, therefore, there is upper limit for Sr doping to avoid excessive reduction in curie point. Data given in table 6.4 is useful in evaluation of overall change in dielectric and piezoelectric properties in 9% Sr doped PZT with ageing time and the effect of heating at 100°C to stabilize the properties. It is not the ageing rate that is normally reported in literature. However, no such ageing data is available in literature for 9% Sr doped PZT.

7 Conclusions

1. Lead Zirconate Titanate (PZT) with formulae $Pb_{0.91}Sr_{0.09}(Zr_{0.53}Ti_{0.47})O_3$ was prepared by conventional mixed oxide route exhibiting adequate properties for sonar applications. Properties achieved by sintering at 1200°C for 2 hours in lead rich atmosphere were Dielectric Cosntant (K) = 1440, Tangent Loss (Tanδ) = 0.0062, Charge Coefficient(d_{33}) = 335 pC/N, Coupling Coefficient (k) = 0.37 and density = 7.55 g/cm^3.
2. An isovalent substituted PZT with 9 % Sr produced higher values of dielectric constant and charge coefficient (d_{33}) than the reported values for PZT with 6 % Sr doping.
3. Dense structure (95% of theoretical density) with grain size 2-3 μm was observed by sintering at 1200°C for 02 hours.
4. Change in properties observed after heating at 100°C was as follows. Coupling Coefficient (k) decreased by 1.5%, Charge Coefficient (d_{33}) decreased by 3.5%, Dielectric Constant (K) decreased by 1%, Dielectric Loss(Tanδ) increased by 2.5% which are much lower than the change occurred when the material was not stabilized (i-e: k decreased by 9.5%, d_{33} decreased by 13.5%, K decreased by 1% and Tanδ increased by 12%).
5. In sintered+poled condition the reflection (002) has higher intensity than reflection (200) due to 90° domain switching whereas in sintered+poled+ground

condition these two reflections exhibit opposite trends indicating that the grinding has the same effect as of annealing.

6. XRD analysis identified starting raw materials: TiO_2 as anatase phase, ZrO_2 as monoclinic phase, PbO as massicot phase and $SrCO_3$ as orthorhombic phase. However; rutile TiO_2 and litharge PbO are considered better phases for PZT fabrication.
7. Laser particle size analyzer revealed that precursor ZrO_2 powder (0.53μm) was coarser than precursor TiO_2 powder (0.18 μm) which could cause compositional fluctuation in the final PZT phase. To counter the difference in reactivity between the two caused by particle size difference, the precursor powders were ground and mixed for longer times (11 hours) in a planetary mill.
8. EDX analysis showed deficiency of Pb in the final sintered product despite the fact that 2.5% extra PbO was added in the initial mixture to compensate lead losses during sintering at 1200°C.

8 Future Suggestions

1. In the present work, the procedure adopted to control the evaporation of PbO was not perfect. A more scientific study is required to control PbO loss by applying thermodynamic calculations to estimate overall evaporation in complete calcination and sintering cycle and then evaluate the PbO loss by experimentation. Or this loss could be monitored and quantified by placing a mass spectrometer at the outlet of sealed box containing the pellet to be calcined and sintered.
2. Compressive stresses perpendicular to the poling direction can be applied to enhance 90° domain switching when the samples are being poled which results in enhancement of charge constant (d_{33}).[57]
3. Enhancement of the piezoelectric effect in bulk ceramics can be accomplished by inducing preferred orientation through grain-orientation processes such as hot forging or tape casting that precede the electrical-poling process.[58]

9 References

[1]C. A. Harper, Electronic Materials and Process Handbook. Third Edition. McGraw-Hill Companies, 2004.

[2]B. Jaffe, W. R. Cook and H Jaffe. Piezoelectric ceramics, Academic Press, New York. 1971.

[3]G. Shirane, K. Suzuki, and A. Takeda, "Phase Transitions in Solid Solutions of Lead Zirconate and Lead Titanate: II," *J. Phys. Soc. Jpn.*, 7 [1] 12–18 (1952).

[4]B. Jaffe, R. S. Roth, and S. Marzullo, "Piezoelectric Properties of Lead Zirconate–Lead Titanate Solid-Solution Ceramics," *J. Appl. Phys.*, 25 [6] 809– 10 (1954).

[5]R. P. Brodeur, K. Gachigi, P. M. Pruna, and T. R. Shrout, "Ultra-High Strain Ceramics with Multiple Field-Induced Phase Transitions," *J. Am. Ceram. Soc.*, 77 [11] 3042–44 (1994).

[6]G. Goodman, "Ceramic Capacitor Materials"; pp. 79–138 in *Ceramic Materials for Electronics*. Edited by R. C. Buchanan. Marcel Dekker, New York, 1986.

[7]R. Manczok and R. Wernicke, "Ceramic Boundary-Layer Capacitors," *Philips Tech. Rev.*, 41 [11/12] 338–46 (1983).

[8]G. H. Haertling, "Ferroelectric Ceramics: History and Technology *J.Am. Ceram. Soc*., 82 [4] 797–818 (1999).

[9]C. Bedoya, C. Muller, J. L. Baudour, V. Madigou, M. Anne, and M. Roubin, "Sr-Doped Pb $Zr_{1-x}Ti_x O_3$ Ceramics: Structural Study and Field-Induced Reorientation of Ferroelectric Domains," *Mater. Sci. Eng*., B75, 43–52 (2000).

[10]H. Zheng, I. M. Reaney, W.E. Lee, N. Jones and H. Thomas, "Effect of strontium substitution in Nb-doped PZT ceramics" J. *Eur. Ceram. Soc*. 21(2001) 1371-1375.

[11]H. Zheng, I. M. Reaney, W. E. Lee, N. Jones and H. Thomas "Surface Decomposition of Strontium-Doped Soft $PbZrO_3$–$PbTiO_3$" *J. Am. Ceram. Soc*., 85 [1] 207–12 (2002).

[12]Ad-hoc submitted report on Piezoceramics: Revision of Dod-Std 1376 A, Orlando, NRL Memorandum Report 5687, Naval Research Laboratory, Underwater Sound Reference Detachment, United States, April 1986.

[13]S. Sirilomask, W. A. Schulze, S. M. Pilgrim and F. A. William Jr., "Harmonic analysis of polarization hysteresis of Aged PZTs *J. Am. Ceram. Soc.,* 88 [8] 2121–2135 (2005).

[14]C. A. Randall, Namchul Kim, John-Paul Kucera, Wenwu Cao and Thomas R. Shrout, "Intrinsic and Extrinsic Size Effects in Fine-Grained Morphotropic-Phase-Boundary Lead Zirconate Titinate Ceramics". *J. Am.Ceram. Soc.,* 81 [3] 677–688(1998).

[15]C. E. Baumgartner, "Fast fiing and conventional sintering of lead zirconate Titinate Ceramic" *J. Am. Ceram. Soc.,* 71 [7] C-350-C-353 (1988).

[16]C. C. Hsueh, M. L. Mecartney, W. B. Harrison, M. R B. Hanson and B. G. Keopke, "Microstructure and electrical properties of fast-fired lead-zirconate-titinate ceramics", *J. Mat. Sci. Letters* 8 (1989) 1209-1216.

[17]A. J. Moulson and J. M. Herbert. Electroceramics Materials , Properties, Applications 2nd Ed. John Wiley and Sons England 2003.

[18]W. F. Smith, "Principles of Materials Science and Engineering" 3rd Edition, McGraw Hill Inc. USA 2004.

[19]Y-M. Chiang, D. Birinie III and W. D. Kingery, "Physical Ceramics: Principles of Ceramic Science and Engineering". MIT series in materials science and engineering. John Wiley and Sons, Inc. USA. 1997.

[20]M. S. Vijaya and G. Rangrgan, Materials Science, Tata McGraw-Hill Publishing company , New Delhi, 2004.

[21]D. Berlincourt, "Piezoelectric ceramic compositional development" *J. Acoust. Soc. Am.*91 (5), May 1992, 3034-3040.

[22]J. Nowotny, Electronic Ceramic Materials. TransTech Publications, Switzerland, 1992.

[23]W. A. Schulze and K. Ogino, "Review of Literature on Aging of Dielectrics," *Ferroelectrics*, 87, 361–77 (1988).

[24]R. C. Bradt and G. S. Ansell, "Aging in Tetragonal Ferroelectric Barium Titanate," *J. Am. Ceram. Soc*., 52 [4] 192–99 (1969).

[25]P. V. Lambeck and G. H. Jonker, "The Nature of Domain Stabilization in Ferroelectric Perovskites," *J. Phys. Chem. Solids*, 47 [5] 453–61 (1986).

[26]K. Okazaki and H. Maiwa, "Space Charge Effects on Ferroelectric Ceramic Particle Surfaces," *Jpn. J. Appl. Phys.*, 31 [9B] 3113–16 (1992).

[27]U. Robels and G. Arlt, "Domain Wall Clamping in Ferroelectrics by Orientation of Defects," *J. Appl. Phys*., 73 [7] 3454–60 (1993).

[28]S-B Kim, D-Y Kim, "Stabilization and Memory of the Domain Structures in Barium TitanateCeramics: Microstructural Observation." *J. Am. Ceram. Soc.,* 83 [6] 1495–98 (2000).

[29]G. H. Haertling, "Piezoelectric and Electrooptic Ceramics"; 135–225 in *Ceramic Materials for Electronics*. Edited by R. C. Buchanan. Marcel Dekker, New York, 1986.

[30]H. Zheng, I. M. Reaney, W. E. Lee, N. Jones and H. Thomas, "Effects of Octahedral Tilting on the Piezoelectric Properties of Strontium/Barium/Niobium-Doped Soft Lead Zirconate Titanate Ceramics" *J. Am. Ceram. Soc.,* 85 [9] 2337–44 (2002).

[31]S-S Chiang, M. Nishioka, R. M. Fulrath and J. A. Pask, "Effect of Processing on Microstructure and properties of PZT ceramics." *Ceramic Bulletin,* Vol., 60, No. 4 (1981) 484-489.

[32]J. Ryu, J-J Choi and H-E Kim, "Effect of heating rate on the sintering behaviuor of Lead Zirconate Ceramics". *J. Am. Ceram. Soc*., 84[4] 902-904 (2001).

[33]A. I. Kingon and J. B. Clark, "Sintering of PZT ceramics: II, "Effect of PbO content on densification kinetics". *J. Am. Ceram. Soc*., Vol 66 No.4 (1983) 256-260.

[34]A. I. Kingon and J. B. Clark, "Sintering of PZT ceramics: I, "Atmoshere Control". *J. Am. Ceram. Soc*., Vol 66 No.4 (1983) 253-256.

[35]K. Kakegawa, O. Matsunaga, T. Kato and Y. Sasaki.,"Compositional change and compositional fluctuation in $Pb(Zr,Ti)O_3$ containing excess PbO" *J. Am. Ceram. Soc.,* 78 [4] 1071-1075 (1995).

[36]A. K. Saha, D. Kumar, O. Prakash, A. Sen, H. S. Maiti, "Effect of phosphorous addition on the sintering and dielectric properties of $Pb(Zr_{0.52}Ti_{0.48})O_3$ *Mater. Res. Bull*. 38 (7) (2003) 1165.

[37]D. L. Corker, R. W. Whatmore, E. Ringgaard, W.W. Wolny, "Liquid Phase Sintering of PZT Ceramics", *J. Eur. Ceram*. Soc 20 (2000) 2039.

[38]Venkataramani and J. V. Biggers, "Reactivity of Zirconia in Calcining of Lead Zirconate-Lead Titanate Compositions Prepared from Mixed Oxides," Am. *Ceram. Soc. Bull.,* 59 [4] 462 (1980).

[39]Lu Y, S. Chen and Li. Q., "Design and Study of a Moonie Pzt Microactutor Slider Driven Device for Hard Disk Drives". IEIC Technical Report (Institute of Electronics, Information and Communication Engineers) Vol.101; No**.** 400(MR2001 54-71); 81-86(2001).

[40]B. L. Theraja, A Textbook of Electrical Technology, Mirja Construction and Development Company Ltd., New Delhi. 1988.

[41]B. D. Cullity and S. R. Stock, Elements of X-Ray Diffraction, 3rd Edition, Prentice-Hall, Inc. New Jersey, USA, 2000.

[42]C. R. Brundle, C. A. Evans, Jr. and S. Wilson, Encyclopedia of materials characterization; surfaces, interfaces, thin films. Butterworth-Heinemann. 1992.

[43]R. M. German. Powder Metallurgy Science, 2nd Edition, MPIF, Princeton New Jersey, USA, 1997.

[44]W. J. Lackey, P. Angelini, A. J. Caputo, C. E. Devore, J . C. Mclaughlin, David P, Stintona, **"**Rate-Controlled Technique for Calcining and Drying", c-102 *Communications of the American Ceramic Society,* June 1984.

[45]S-Y. Chen, S-Y. Cheng, and C-M. Wang, "Polymorphic Phase Transformation of lead monoxide and its influence on Lead Zirconate Titanate Formation *J. Am. Ceram. Soc.,*73 [2] 232-36 (1990).

[46]B.V. Hiremath, A. I. Kingon, and J. V. Biggers, "Reaction Sequence in the Formation of Lead Zirconate-Lead Titanate Solid Solution: Role of Raw Materials," ***J.** Am. Ceram. Soc.,* 66 [ll] 790-93 (1983).

[47]Y. Matsuo and H. Sasaki, "PbO-Rich Side of the System PbO-Ti02," *J. Am. Ceram. Soc.,* 46 [8] 409-10 (1963).

[48]L. B. Kong, J. Ma, "PZT ceramics formed directly from oxides via reactive sintering". *Materials Letters,* 51(2001) 95-100.

[49]T. R Shrout, P. Papet, S. Kim and G-S. Lee, "Conventionally prepared submicrometer lead based perovskite powders by reactive calcinations." *J. Am. Ceram. Soc.,* 73 [7] 1862-67 (1990).

[50]Z. Wang, Q. Jiang, G. S. White and A. K. Richardson, "Processing flaws in PZT transducer rings". *Smart Mater. Struc.* 7 (1998) 873-867.

[51]A. Boutarfaia, C. Boudaren, A. Mousser and S. E. Bouaoud " Study of Phase Transition Line of PZT Ceramics by X-Ray Diffraction" *Ceramics International* 21 (1995) 391-394.

[52]M. Hammer, C. Monty, A. Endriss and M. J. Hoffmann, "Correlation between Surface Texture and Chemical Composition in Undoped, Hard, and Soft Piezoelectric PZT Ceramics" *J. Am. Ceram. Soc.,* 81 [3] 721–24 (1998).

[53]K. Okazaki and K. Nagata,"Effect of Grain Size and Porosity on Electrical and Optical Properties of PLZT Ceramics", *J. Am. Ceram. Soc*., 56(1973) 82.

[54]Z. Zhang and R. Raj, "Influence of grain size on ferroelastic toughening and piezoelectric behaviour of Lead Zirconate Titinate". *J. Am. Ceram. Soc.*, 78 [12] 3363–68 (1995).

[55]S. C. Sharma and R. Lal, ‘‘Microstructure & Properties of Modified Lead Zirconate–Titanate Ceramics,’’ Indian J. Pure Appl. Phys., 27, 171–3 (1989).

[56]H. Wang, S. Cheng, and C. Wang, ‘‘The Initial Aging Behavior of PZT Ceramics’’, pp. 399–408 in Ceramic Transactions, Vol. 8, Ceramic Dielectric Composition; Processing and Properties ’89, Edited by H. C. Ling and M. F. Yan. American Ceramic Society, Westerville, OH, 1989.

[57]J. L. Jones, A. B. Kounga, E. Aulbach and T. Granzowy, “Domain Switching During Electromechanical Poling in Lead Zirconate Titanate Ceramics” *J. Am. Ceram. Soc*., 91 [5] 1586–1590 (2008).

[58]J. L. Jones, B. J. Iverson and K. J. Bowmanw, “Texture and Anisotropy of Polycrystalline Piezoelectrics” *J. Am. Ceram. Soc*., 90 [8] 2297–2314 (2007).